Cosmological phase transitions at three loops: The final verdict on perturbation theory

Ekstedt, Andreas; Schicho, Philipp; Tenkanen, Tuomas V.I.

How to cite

EKSTEDT, Andreas, SCHICHO, Philipp, TENKANEN, Tuomas V.I. Cosmological phase transitions at three loops: The final verdict on perturbation theory. In: Physical review. D., 2024, vol. 110, n° 9, p. 096006. doi: 10.1103/physrevd.110.096006

This publication URL: https://archive-ouverte.unige.ch/unige:183034
Publication DOI: 10.1103/physrevd.110.096006

Cosmological phase transitions at three loops: The final verdict on perturbation theory

Andreas Ekstedt,[1,*] Philipp Schicho,[2,3,†] and Tuomas V. I. Tenkanen[4,5,6,7,‡]

[1]*Department of Physics and Astronomy, Uppsala University, Box 516, SE-751 20 Uppsala, Sweden*
[2]*Département de Physique Théorique, Université de Genève, 24 quai Ernest Ansermet, CH-1211 Genève 4, Switzerland*
[3]*Institute for Theoretical Physics, Goethe Universität Frankfurt, 60438 Frankfurt, Germany*
[4]*Department of Physics and Helsinki Institute of Physics, P.O. Box 64, FI-00014 University of Helsinki, Finland*
[5]*Nordita, KTH Royal Institute of Technology and Stockholm University, Hannes Alfvéns väg 12, SE-106 91 Stockholm, Sweden*
[6]*Tsung-Dao Lee Institute & School of Physics and Astronomy, Shanghai Jiao Tong University, Shanghai 200240, China*
[7]*Shanghai Key Laboratory for Particle Physics and Cosmology, Key Laboratory for Particle Astrophysics and Cosmology (MOE), Shanghai Jiao Tong University, Shanghai 200240, China*

(Received 11 June 2024; accepted 24 September 2024; published 6 November 2024)

We complete the perturbative program for equilibrium thermodynamics of cosmological first-order phase transitions of gauge-Higgs theories that map into the (three-dimensional) superrenormalizable SU(2) + doublet effective theory at high temperatures. To this end, we determine their finite-temperature effective potential at next-to-next-to-next-to-next-to-leading order (N^4LO). The computation of the three-loop effective potential required to reach this order is also presented for U(1) gauge theories and is readily extendable to generic models in dimensionally reduced effective theories. Our N^4LO result is the last perturbative order before confinement renders electroweak gauge-Higgs theories nonperturbative at four loops. By contrasting our analysis with nonperturbative lattice results, we find a remarkable agreement. As a direct application for predictions of gravitational waves produced by a first-order transition, our computation provides the final fully perturbative results for the phase transition strength and speed of sound.

DOI: 10.1103/PhysRevD.110.096006

I. INTRODUCTION

Phase transitions are milestones in the early Universe—be it by triggering inflation [2,3], sparking baryogenesis [4–6], or creating a symphony of gravitational waves [7–11]. Such transitions typically occur at high temperatures and their properties are often difficult to predict reliably. Especially for gravitational-wave (GW) production, where theoretical calculations can misjudge the peak amplitude by ten orders of magnitude [12]. And with next-generation GW experiments—LISA [13], DECi-hertz Interferometer GW Observatory (DECIGO) [14,15], Big Bang Observer [16], TAIJI [17], and TIANQIN [18]—on the horizon, it is clear that theoretical predictions are not yet up to par. As such there is a drive to improve the predictions and augment conventional frameworks [19–24] with state-of-the-art tools. The tool in question is effective field theory (EFT) [25–28].

These theoretical difficulties manifest when considering GW production during a primordial phase transition. As the universe cools down, first-order phase transitions occur by nucleating bubbles of the new phase within the old one. For the electroweak case, an extended Higgs sector is required to render the transition first-order; in which case these bubbles release an enormous amount of latent heat and are rapidly accelerated. As bubbles collide and generate sound waves, a quadrupole moment is induced, which subsequently sources gravitational waves. The production and propagation of bubbles in a first-order phase transition is a classical process. It occurs on length scales much larger

*Contact author: andreas.ekstedt@physics.uu.se
†Contact author: philipp.schicho@unige.ch
‡Contact author: tuomas.tenkanen@helsinki.fi

than the temperature, *viz.* $L \gg T^{-1}$, while in the fundamental theory quantum fluctuations dominantly occur at $L \sim T^{-1}$. Conversely, making *classical* predictions directly within the *quantum* theory leads to a host of problems. These problems include the presence of large loop corrections and ad-hoc recipe for calculating thermodynamic and dynamic quantities; see the discussions in [28,29].

A rigorous solution is to make all predictions directly within a classical theory. To this end, quantum fluctuations with a characteristic energy $E \sim T$, are encoded in the classical theory as effective parameters. Since equilibrium dynamics is, by definition, time-independent, the effective classical theory is static and fields only depend on three-dimensional (3D) spatial coordinates. Thus the name dimensional reduction [30,31]. Thermally induced bubble nucleation is also a classical process and the rate of nucleation, Γ, is set by the energy-cost of nucleating a bubble at rest, $\Gamma \sim e^{-E_{\rm bubble}/T}$. This energy is again a static quantity, calculable within the dimensionally reduced theory (3D EFT). The construction of such 3D EFTs is a well-understood, purely perturbative process with ample applications beyond the Standard Model (SM) [12,32–45].

By computing Feynman diagrams such 3D EFTs can be studied perturbatively. At least up to a fixed loop order. One complication is that 3D field theories are confining which results in glueball-like bound states that become important at high enough loop orders, which necessitates lattice simulations [32,46–53]. For SU(N) gauge theories, nonperturbative effects become important at four loops. Intuitively, such nonperturbative effects are related to the logarithmic dependence of the vector potential in $(2+1)$ dimensions,[1] $V(r) \approx g^2 T \ln r$, where g is a generic coupling constant. This gives rise to bound-states with a characteristic mass $m_{\rm M} \sim r_{\rm c}^{-1} \sim g^2 T$ and the emergence of confinement at a scale $r_{\rm c}$. In the broken-Higgs phase this is not an issue as $(g\phi)^{-1} \ll r_{\rm c}$ for a nonzero classical scalar background ϕ. In the symmetric phase, however, gauge-boson fluctuations are controlled by the magnetic mass $m_{\rm M}$. Since the free-energy has units of mass cubed in 3D, the nonperturbative contribution is of the order $F_{\rm free}^{\rm nonpert} \sim m_{\rm M}^3 \sim g^6 T^3$ in the symmetric phase. This is the same order as four-loop diagrams in the broken phase. Thus nonperturbative contributions can only be ignored up to three loops.

Alternatively, in the original argument by Linde [54], such a breakdown of perturbation theory can be seen directly by estimating the size of higher-order loops. Since the free-energy within the 3D theory is computed via ℓ-loop vacuum diagrams linked by $\ell - 1$ vertices with 3D coupling $g_3^2 \sim g^2 T$ and by $2\ell - 2$ propagators with mass $m_{\rm M}$ (using here $m_{\rm M}$ for dimensional reasons), the ℓ-loop integration in 3D yields $m_{\rm M}^{3\ell}$ and renders the overall diagram proportional to $g_3^6 (g_3^2/m_{\rm M})^{\ell-4}$. Consequently, a magnetic-scale mass $m_{\rm M} \sim g^2 T$ contributes at $\mathcal{O}(g^6 T^3)$ *irrespective* of the loop order ℓ. This results in a problem deep in the infrared (IR), while modes with masses $m \gg m_{\rm M}$ can still be treated perturbatively.

The perturbative program aims to determine all perturbative orders before facing the IR problem. In hot QCD, this program has a long history. While the leading-order (LO) pressure p_0 is described by the Stefan-Boltzmann law, perturbative corrections to the pressure p/p_0 were computed at $\mathcal{O}(g^2)$ [55], $\mathcal{O}(g^3)$ [56], $\mathcal{O}(g^4 \ln \frac{1}{g})$ [57], $\mathcal{O}(g^5)$ [58,59]. The final perturbative $\mathcal{O}(g^6 \ln \frac{1}{g})$ was achieved already two decades ago [60]. At this final order, also massless O(N) scalar field theories were studied perturbatively [61,62], and nonperturbatively using numerical methods [63,64].

This *article* pushes the perturbative program in electroweak theories to its limit by studying the phase structure of SU(2) and U(1) Higgs-gauge theories at three loops.[2] This endeavor is powered by EFT techniques combined with the renormalization group, which allows for an all-order resummation of leading logarithms [71]. We have also automated the three-loop calculations for generic models, which together with the technical details are relegated to a companion paper [1]. Analytic, three-loop, results are provided for scalar condensates and critical mass which in turn can be related to the phase transition latent heat and critical temperature. We also compare our results with lattice Monte-Carlo simulations [72], and find that three-loop corrections significantly improve the agreement with the lattice in the perturbative regime.

The *article* is organized as follows. Section II defines the effective theory of interest and describes the organization of the three-loop computation. Section III presents the results for the critical mass and scalar condensates and compares the analytic results to previous nonperturbative lattice simulations. In Sec. IV, we apply our computation to illuminating setups of dark sector phase transitions and discuss the impact of higher-order corrections to GW predictions. We summarize our findings in Sec. V and discuss future directions. Appendix A organizes the broken-phase perturbative series. Appendix B collects the thermodynamic results for the Abelian Higgs model. Appendix C details the EFT construction for a simplified model.

II. THREE-LOOP COMPUTATION

The construction of dimensionally reduced effective theories from generic parent theories is detailed in [27], and further automated in [41]. Here, we directly start with the three-dimensional theory action

[1] In $(d-1)+1$-dimensions, the potential behaves as r^{3-d}.

[2] For SU(N)+ adjoint Higgs theory, which is the relevant EFT of QCD, similar perturbative computation reached four-loop level [65]; cf. also [66–70].

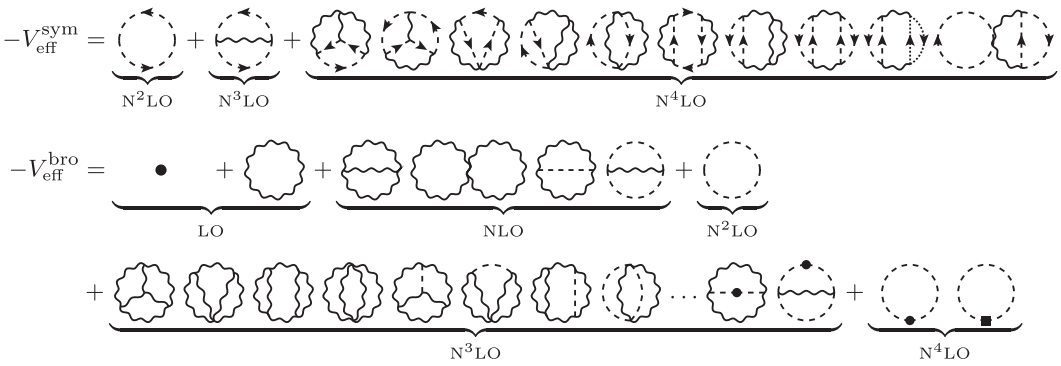

FIG. 1. Diagrams contributing to the symmetric- and broken-phase effective potential up to N^{4}LO. In the symmetric phase, wiggly lines denote SU(N) vector bosons A_μ^a, directed dotted lines ghosts, and directed dashed lines the Higgs N-tuplet, Φ. In the broken phase and for SU(2), wiggly lines denote the vectors bosons Z, $W^\pm$, and dashed lines scalars $h, G, G^\pm$. Blobs correspond to mass and boxes to field renormalization insertions of eqs. (20)–(21). The diagrams were drawn with AXODRAW [75].

$$S_3 = \int_{\mathbf{x}} \left[\frac{1}{4} F_{ij}^a F_{ij}^a + (D_i\Phi)^\dagger (D_i\Phi) + V(\Phi) \right], \quad (1)$$

where $\int_{\mathbf{x}} = \int \mathrm{d}^d x$ and $d = 3 - 2\epsilon$. The gauge coupling is denoted as g_3 inside the covariant derivative $D_i\Phi = (\partial_i - i g_3 A_i)\Phi$, where $A_i = A_i^a T^a$ and T^a are the generators of SU(N) under which the scalar Φ transforms as an N-tuplet. For the broken phase, we focus on the case where Φ transforms as a doublet under SU(2) and, in Appendix B, as a singlet under U(1). For the symmetric phase, we retain a general N. The tree-level potential is

$$V(\Phi) = m_3^2 \Phi^\dagger \Phi + \lambda_3 (\Phi^\dagger \Phi)^2, \quad (2)$$

with the scalar mass parameter squared m_3^2 and scalar self-coupling λ_3. The subscript on these couplings reminds us that these are effective parameters of the 3D EFT, and that they have dimension of mass. While Eq. (1) describes the Standard Model at high temperatures and vanishing hypercharge coupling, many Standard Model extensions also map to this theory due to its universal character, albeit with different values of couplings. An example of such a mapping is shown in Appendix C. Throughout our analysis, we assume that Eq. (1) does not include any higher-dimensional, marginal operators such as $(\Phi^\dagger\Phi)^3$. Given this assumption, we complete the perturbative program for equilibrium thermodynamics for a class of models that map into this specific EFT in the infrared [Eq. (1)]. This allows for directly comparing with earlier nonperturbative lattice studies of the same model. In our companion article [1], we generalize our computations to other types of models.

The potential in Eq. (2) does not exhibit a barrier. However, a barrier can be generated if the vector-boson mass is large. For this to happen, vector-boson induced loops need to be comparable with the tree-level potential. Formally, the vector bosons can be integrated out in the broken phase. In the symmetric phase, where vector bosons are massless, the full theory must be considered.

As a consequence, the LO broken-phase action for SU(2) contains only scalar fields [73,74]

$$S_{\rm LO} = \int_{\mathbf{x}} \left[(\partial_i\Phi)^\dagger (\partial_i\Phi) + V_{\rm LO}(\Phi) \right],$$
$$V_{\rm LO}(\Phi) = m_3^2 \Phi^\dagger\Phi + \lambda_3 (\Phi^\dagger\Phi)^2 - \frac{g_3^3}{2\pi} \left(\frac{\Phi^\dagger\Phi}{2} \right)^{3/2}. \quad (3)$$

We remark that this construction only works if $m_3^2/m_{\rm A}^2 \sim \lambda_3/g_3^2 \ll 1$, where $m_{\rm A} \sim g_3\phi$ is the broken-phase vector-boson mass and $m_3^2 \sim \lambda_3\phi^2$. The LO potential in Eq. (3) then admits a first-order transition, and therefore serves as a good starting point for a perturbative treatment.

Adding perturbative corrections can be guided by assigning a power counting for EFT parameters in terms of a formal counting parameter g of an underlying parent theory with temperature T [74] [3]

$$m_3^2 \sim g^3 T^2, \qquad \lambda_3 \sim g^3 T, \qquad g_3^2 \sim g^2 T. \quad (4)$$

Then, the effective potential can be expanded as

$$\frac{V_{\rm eff}}{T^3} \sim \underbrace{\boxed{g^3}}_{\rm LO} + \underbrace{\boxed{g^4}}_{\rm NLO} + \underbrace{\boxed{g^{9/2}}}_{\rm N^2LO} + \underbrace{\boxed{g^5}}_{\rm N^3LO} + \underbrace{\boxed{g^{11/2}}}_{\rm N^4LO} + \mathcal{O}(g^6). \quad (5)$$

As mentioned in the introduction, $\mathcal{O}(g^6)$ terms require nonperturbative input. To compute the effective potential, we first keep g as an expansion parameter before later choosing a more appropriate expansion parameter in the 3D theory. Concretely and as depicted in Fig. 1, the first five

[3] This assignment ties together the scalings of EFT parameters, and only assumes that the formal expansion parameter of a parent theory is g^2, cf. [74].

orders of Eq. (5) originate from

$V_{\rm eff}^{\rm LO} \sim g^3$ Tree-level scalar and one-loop vector,
$V_{\rm eff}^{\rm NLO} \sim g^4$ Two-loop vector,
$V_{\rm eff}^{\rm N^2LO} \sim g^{\frac{9}{2}}$ One-loop scalar,
$V_{\rm eff}^{\rm N^3LO} \sim g^5$ Three-loop vector and subleading, two-loop vector-scalar,
$V_{\rm eff}^{\rm N^4LO} \sim g^{\frac{11}{2}}$ Subleading one-loop scalar.

For the symmetric-phase potential, multiple diagrams contribute as depicted in Fig. 1. While for the first two orders at leading and next-to-leading order (NLO) $V_{\rm eff}|^{\rm sym}_{\rm LO} = V_{\rm eff}|^{\rm sym}_{\rm NLO} \equiv 0$, the first nonvanishing contributions arise at next-to-next-to-leading order (N^2LO), next-to-next-to-next-to-leading order (N^3LO), and next-to-next-to-next-to-next-to-leading order (N^4LO), *viz.*

$$V_{\rm eff}|^{\rm sym}_{\rm N^2LO} = -\frac{N}{6\pi}(m_3^2)^{\frac{3}{2}}, \tag{6}$$

$$V_{\rm eff}|^{\rm sym}_{\rm N^3LO} = -\frac{g_3^2 m_3^2}{(4\pi)^2}\frac{NC_{\rm F}}{2}\left[-3+4\ln 2+2\ln\frac{m_3^2}{\bar{\mu}_3^2}\right], \tag{7}$$

$$\begin{aligned} V_{\rm eff}|^{\rm sym}_{\rm N^4LO} = {} & \frac{g_3^4 C_{\rm F}}{(4\pi)^3}(m_3^2)^{\frac{1}{2}}\left[\frac{81N^2+10N-87}{24}+\frac{NC_{\rm F}}{3}\pi^2\right. \\ & +\frac{12N^2-7N+27}{6}\ln 2 \\ & \left.+\frac{4N^2-N+3}{4}\ln\frac{m_3^2}{\bar{\mu}_3^2}\right], \end{aligned} \tag{8}$$

computed in general R_ξ (or Fermi) gauge; see [76] for the generalized gauge fixing. Here, $\bar{\mu}_3$ is the 3D renormalization scale and $C_{\rm F} = (N^2-1)/(2N)$ is the Casimir operator in the fundamental representation. The full SU(N) Standard-Model symmetric pressure including adjoint (temporal) scalars is given by [77–79].

The two-loop β-functions for the mass and the vacuum running, using $t_3 = \ln\bar{\mu}_3$, are

$$\begin{aligned} \partial_{t_3} m_3^2 = {} & -\frac{2}{(4\pi)^2}\frac{1}{N}\left[\frac{C_{\rm F}(4N^2-N+3)}{4}g_3^4\right. \\ & \left.+2N(N+1)\left(C_{\rm F}g_3^2\lambda_3-\lambda_3^2\right)\right], \end{aligned} \tag{9}$$

$$\partial_{t_3} V_0 = -2NC_{\rm F}\frac{g_3^2 m_3^2}{(4\pi)^2}, \tag{10}$$

where the field-independent $V_0 = V|_{\Phi=0}$. Since the 3D EFT is super-renormalizable [71], the mass β-function is exact, while the vacuum β-function will also receive a four-loop contribution. The potential $V_{\rm eff}|^{\rm sym}$ is renormalization-scale independent to the computed order. The running at N^2LO, using Eq. (9), is canceled by the explicit logarithm at N^4LO, and the explicit logarithm at N^3LO is canceled by the vacuum running of Eq. (10).

After splitting the scalar field into $\Phi \to \frac{1}{\sqrt{2}}\phi\delta_{i,N} + \Phi$, the broken-phase effective potential is composed of the diagrammatic contributions given in Fig. 1. Henceforth, we focus on SU(2), for which the broken-phase potential amounts to

$$V_{\rm eff}|^{\rm bro}_{\rm LO} = \frac{1}{2}m_3^2\phi^2 + \frac{1}{4}\lambda_3\phi^4 - \frac{1}{16\pi}g_3^3\phi^3, \tag{11}$$

$$V_{\rm eff}|^{\rm bro}_{\rm NLO} = \frac{g_3^4\phi^2}{(16\pi)^2}\frac{3}{4}\left[11-42\ln\frac{3}{2}+34\ln\frac{\bar{\mu}_3}{g_3\phi}\right], \tag{12}$$

$$V_{\rm eff}|^{\rm bro}_{\rm N^2LO} = -\frac{1}{12\pi}\left[\tilde{m}_h^3+3\tilde{m}_{\rm G}^3\right], \tag{13}$$

$$\begin{aligned} V_{\rm eff}|^{\rm bro}_{\rm N^3LO} = {} & \frac{3g_3^2}{(16\pi)^2}\left[m_3^2\left(5+12\ln 2+16\ln\frac{\bar{\mu}_3}{g_3\phi}\right)\right. \\ & \left.+3\lambda_3\phi^2\left(3+4\ln 2+8\ln\frac{\bar{\mu}_3}{g_3\phi}\right)\right] \\ & +\frac{g_3^5\phi}{(16\pi)^3}\aleph_{\text{\Large$\circ$}}, \end{aligned} \tag{14}$$

$$\begin{aligned} V_{\rm eff}|^{\rm bro}_{\rm N^4LO} = {} & -\frac{g_3}{(16\pi)^2}\frac{2}{\phi}\left[11\tilde{m}_h^3+48\tilde{m}_{\rm G}^3\right] \\ & +\frac{6g_3^4}{(16\pi)^3}\left[\tilde{m}_h\left(20+21\ln\frac{3}{2}-17\ln\frac{\bar{\mu}_3}{g_3\phi}\right)\right. \\ & \left.+3\tilde{m}_{\rm G}\left(3+21\ln\frac{3}{2}-17\ln\frac{\bar{\mu}_3}{g_3\phi}\right)\right], \end{aligned} \tag{15}$$

computed in Landau gauge.[4] The three-loop constant used above is defined as

$$\begin{aligned} \aleph_{\text{\Large$\circ$}} \equiv {} & \frac{801}{2}+\frac{1843}{32}\pi^2+2643\ln 2-\frac{2943}{2}\ln 3-\frac{8361}{16}\ln^2 3 \\ & -\frac{7353}{4}\left(\ln^2 2-\ln 2\ln 3+\frac{1}{2}\mathrm{Li}_2\left(\frac{1}{4}\right)\right)-63\mathrm{Li}_2\left(\frac{1}{3}\right) \\ & -\frac{849}{2\sqrt{2}}\left(\mathrm{Ls}_2(4\alpha)-\mathrm{Ls}_2(2\alpha)\right) \\ \approx {} & 791.9306523639452(1), \end{aligned} \tag{16}$$

[4]Throughout this *article*, we use a gauge-invariant method and explicitly verified the gauge-invariance of most contributions; barring some three-loop diagrams where we only used Landau gauge.

where $\alpha = \arcsin\frac{1}{3}$. Due to the vector Mercedes diagram () [80], it contains the transcendental functions for the polylogarithm $\mathrm{Li}_s(z)$ and log-sine integral

$$\mathrm{Ls}_j(\theta) = -\int_0^\theta \mathrm{d}\tau \ln^{j-1}\left|2\sin\frac{\tau}{2}\right|, \tag{17}$$

where $\mathrm{Ls}_2(\theta) = \frac{1}{2i}(\mathrm{Li}_2(e^{i\theta}) - \mathrm{Li}_2(e^{-i\theta}))$.

The resummed scalar masses for Higgs and Goldstone bosons in the EFT are

$$\tilde{m}_h^2(\phi) = \partial_\phi^2 V_{\mathrm{LO}}, \qquad \tilde{m}_{\mathrm{G}}^2(\phi) = \phi^{-1}\partial_\phi V_{\mathrm{LO}}, \tag{18}$$

$$\Pi_h(\phi) = \partial_\phi^2 V_{\mathrm{NLO}}, \qquad \Pi_{\mathrm{G}}(\phi) = \phi^{-1}\partial_\phi V_{\mathrm{NLO}}, \tag{19}$$

where we treat higher-order corrections perturbatively.

The N^{3}LO and N^{4}LO potential comes from a direct computation of three-loop diagrams in Fig. 1. The N^{4}LO potential can also be found by using the background-field method [81–83], and we have verified that the two methods agree. The direct three-loop computation is detailed in the companion paper [1] and was conducted in R_ξ gauge [76] for the symmetric-phase and Landau gauge for the broken phase. This computation uses both FEYNCALC [84] and FIRE [85]; as well as in-house FORM [86] software for Feynman diagram computations after their generation with QGRAF [87] and for three-loop integration-by-parts (IBP) identities such as in [88].

For simplicity, we illustrate the background-field derivation. By integrating out the vector-boson field in the scalar-field background, corrections to the mass, coupling, and kinetic terms are generated. In turn, these corrections produce the N^{4}LO potential. For example, inserting the NLO mass corrections and field renormalization in the one-loop scalar diagram as in Fig. 1, gives


$$= -\frac{C_s}{2}\Pi_s(\phi)\int_{\mathrm{p}}\frac{1}{p^2+\tilde{m}_s^2}, \tag{20}$$


$$= \frac{C_s}{2}\bar{\Pi}_s(\phi)\tilde{m}_s^2\int_{\mathrm{p}}\frac{1}{p^2+\tilde{m}_s^2}, \tag{21}$$

where a summation over $s = \{h, G\}$ is implied and where $C_s = 1$ for the Higgs and $C_s = 3$ for Goldstones. The field renormalization corrections, $Z_s = 1 + \bar{\Pi}_s$, are

$$\bar{\Pi}_h = -\frac{11}{16\pi}\frac{g_3}{\phi}, \qquad \bar{\Pi}_{\mathrm{G}} = -\frac{1}{\pi}\frac{g_3}{\phi}. \tag{22}$$

This leads to a k-momentum-dependent effective two-point vertex $\int_x(\partial_i s)Z_s \to -k^2\bar{\Pi}_s$ giving rise to the N^{4}LO contribution of Eq. (21).

Using the β-functions of Eqs. (9) and (10), one can confirm that the effective potential, V_{eff}, is renormalization-scale invariant to the compute order. The running at LO cancels explicit logarithms at NLO and N^{3}LO, and the running of N^{2}LO is compensated by explicit logarithms at N^{4}LO. Vacuum running also cancels mass-dependent scale dependence at N^{3}LO.

Contributions of $\mathcal{O}(g^6\ln g)$ appear at the four-loop level and have been computed in electrostatic QCD [60,65]. Such contributions can also be included without an actual four-loop computation by utilizing renormalization-scale invariance of the effective potential, i.e., $\partial_{t_3}V_{\mathrm{eff}} = 0$, and the fact that the 3D EFT is superrenormalizable and its running known exactly. For SU(2) with a doublet scalar, this $\mathcal{O}(g^6)$ contribution (including logarithms) is

$$V_{\mathrm{eff}}\big|^{\mathrm{sym}}_{\mathrm{N^5LO}} = +\frac{1}{(4\pi)^4}\left[\mathcal{A} + \frac{153}{128}g_3^6\ln\frac{m_3^2}{\bar{\mu}_3^2} \times\left(-1+4\ln 2+\ln\frac{m_3^2}{\bar{\mu}_3^2}\right)\right], \tag{23}$$

$$V_{\mathrm{eff}}\big|^{\mathrm{bro}}_{\mathrm{N^5LO}} = -\frac{3\phi^2\lambda_3^2}{(4\pi)^2}\left(1+\ln\frac{\bar{\mu}_3}{3\tilde{m}_h}+\ln\frac{\bar{\mu}_3}{3\tilde{m}_{\mathrm{G}}}\right) + \frac{1}{(4\pi)^4}\left[\mathcal{B}+\frac{153}{256}g_3^6\ln\frac{\bar{\mu}_3}{g_3\phi} \times\left(5+12\ln 2+8\ln\frac{\bar{\mu}_3}{g_3\phi}\right)\right]. \tag{24}$$

The coefficients $\mathcal{A}$ and $\mathcal{B}$ are determined through a genuine four-loop computation and they are functions of m_3^2, g_3, λ_3, and ϕ but, crucially, do *not* involve logarithms. The N^{5}LO broken-phase potential can also be expressed diagrammatically and would compose of four-loop gauge-scalar diagrams with vanishing scalar masses, two- and three-loop gauge-scalar diagrams with scalar mass insertions, and pure scalar two-loop sunset diagrams, in analogy to Fig. 1. Diagrams with mass insertions are ultraviolet (UV) finite and do not involve a logarithmic dependence, i.e., they are captured by $\mathcal{B}$. Since perturbative contributions do not fully describe the N^{5}LO due to nonperturbative physics (cf. [70,89]), we do not include these corrections in our analysis. In the pure IR scalar sector, all one-loop diagrams with higher-order mass and kinetic insertions contribute at the next order, $\mathcal{O}(g^{\frac{13}{2}})$, and are hence absent in Eq. (23).

The free-energy of the broken phase is obtained by formally expanding the potential around the LO minimum

$$\begin{aligned}F_{\mathrm{bro}} = V_{\mathrm{eff}}(\phi_{\mathrm{min}}) &= V_{\mathrm{eff}}|_{\mathrm{LO}} + V_{\mathrm{eff}}|_{\mathrm{NLO}} + V_{\mathrm{eff}}|_{\mathrm{N^2LO}} \\ &+ \left(V_{\mathrm{eff}}|_{\mathrm{N^3LO}} + \phi_1 V'_{\mathrm{eff}}|_{\mathrm{NLO}} + \frac{1}{2}\phi_1^2 V''_{\mathrm{eff}}|_{\mathrm{LO}}\right)_{\mathrm{N^3LO}} \\ &+ \left(V_{\mathrm{eff}}|_{\mathrm{N^4LO}} + \phi_2 V'_{\mathrm{eff}}|_{\mathrm{NLO}} \right. \\ &\left. + \phi_1 V'_{\mathrm{eff}}|_{\mathrm{N^2LO}} + \phi_1\phi_2 V''_{\mathrm{eff}}|_{\mathrm{LO}}\right)_{\mathrm{N^4LO}},\end{aligned} \tag{25}$$

where primes denote derivative with respect to background field. The minimum is expanded formally as $\phi_{\rm min} = [\phi_0 + \phi_1 + \phi_2 + \ldots]$ and all terms are evaluated at the LO minimum

$$\phi_0 = \frac{3g_3^3 + \sqrt{9g_3^6 - 1024\pi^2\lambda_3 m_3^2}}{32\pi\lambda_3}, \tag{26}$$

and where

$$\phi_1 \equiv -\frac{V'_{\rm eff}|_{\rm NLO}}{V''_{\rm eff}|_{\rm LO}}, \qquad \phi_2 \equiv -\frac{V'_{\rm eff}|_{\rm N^2LO}}{V''_{\rm eff}|_{\rm LO}}, \tag{27}$$

are evaluated at ϕ_0.

As a practical step, rescaling the fields $\Phi \to g_3\Phi$ and the potential in Eq. (3) as $V_{\rm LO}(\Phi) \to g_3^{-6}V_{\rm LO}(\Phi)$, gives

$$V_{\rm LO}(\Phi) \to y\Phi^\dagger\Phi + x(\Phi^\dagger\Phi)^2 - \frac{1}{2\pi}\left(\frac{\Phi^\dagger\Phi}{2}\right)^{3/2}. \tag{28}$$

Below we also rescale $\bar{\mu}_3 \to g_3\bar{\mu}_3$. As a result, the theory is characterized by two dimensionless couplings

$$x \equiv \frac{\lambda_3}{g_3^2}, \qquad y \equiv \frac{m_3^2}{g_3^4}. \tag{29}$$

In the following, the perturbative series will be organized in powers of $x \ll 1$ since $y \sim x^{-1}$ in the vicinity of the phase transition. The expansion of the effective potential becomes

$$\frac{V_{\rm eff}}{g_3^6} \sim \underbrace{x^{-3}}_{\rm LO} + \underbrace{x^{-2}}_{\rm NLO} + \underbrace{x^{-\frac{3}{2}}}_{\rm N^2LO} + \underbrace{x^{-1}}_{\rm N^3LO} + \underbrace{x^{-\frac{1}{2}}}_{\rm N^4LO} + \mathcal{O}(1), \tag{30}$$

which reformulates Eq. (5) in terms of an expansion parameter *within* the 3D EFT [73]. This has the advantage that the EFT can be treated independently of any parent theory.

To summarize, at higher orders two types of contributions arise,

(i) full powers of x from integrating out heavy, UV, modes including all vector bosons,
(ii) fractional powers of x from calculating loops with IR modes of the transitioning scalar.

To determine the phase transition critical temperature $T_{\rm c}$, or equivalently critical mass $y_{\rm c}$, we must find the value of y, given x, where the free energies of the two phases coincide:

$$\Delta F(y_{\rm c}(x), x) = [F_{\rm bro} - F_{\rm sym}](y_{\rm c}(x), x) = 0, \tag{31}$$

where for a quantity X, differences between the broken and symmetric phase are henceforth denoted as $\Delta X = X_{\rm bro} - X_{\rm sym}$. The goal is to find $y_{\rm c}$ order by order in x which has the added advantage that observables are manifestly renormalization-scale invariant at every order.

The entropy-difference between the two phases, $\Delta S = \frac{\rm d}{{\rm d}\ln T}\Delta F(y_{\rm c}, x)$, characterizes the amount of heat released by the transition, and thus its strength. In the effective theory all temperature dependence is encoded in the effective couplings. The chain-rule can be used to rewrite temperature derivatives as y and x derivatives [50]

$$\Delta\langle\Phi^\dagger\Phi\rangle \equiv \frac{\partial}{\partial y}\Delta F, \qquad \Delta\langle(\Phi^\dagger\Phi)^2\rangle \equiv \frac{\partial}{\partial x}\Delta F, \tag{32}$$

and express the entropy in terms of so-called *condensates* [46]

$$\Delta S = \left(\frac{{\rm d}y_{\rm c}}{{\rm d}\ln T}\right)\Delta\langle\Phi^\dagger\Phi\rangle + \left(\frac{{\rm d}x}{{\rm d}\ln T}\right)\Delta\langle(\Phi^\dagger\Phi)^2\rangle, \tag{33}$$

where $\langle\Phi^\dagger\Phi\rangle$ is the quadratic scalar condensate and $\langle(\Phi^\dagger\Phi)^2\rangle$, the quartic condensate.

III. RESULTS FOR THE CRITICAL MASS AND SCALAR CONDENSATES

Perturbative results for the critical mass, and the condensates of SU(2) with a fundamental Higgs are known to N^{2}LO [73]

$$y_{\rm c} = \frac{1}{2^3(4\pi)^2 x}\left[1 - \frac{51}{2}x\ln\tilde{\mu}_3 - (2x)^{\frac{3}{2}}\right], \tag{34}$$

$$\Delta\langle\Phi^\dagger\Phi\rangle_{\rm c} = \frac{1}{2^3(4\pi)^2 x^2}\left[1 + \frac{51}{2}x + \frac{13}{2}(2x)^{\frac{3}{2}}\right], \tag{35}$$

$$\Delta\langle(\Phi^\dagger\Phi)^2\rangle_{\rm c} = \frac{1}{2^6(4\pi)^4 x^4}\left[1 + 51x + 7(2x)^{\frac{3}{2}}\right], \tag{36}$$

where $\tilde{\mu}_3 \equiv e^{\frac{11}{34}-\frac{42}{34}\ln\frac{3}{2}}(8\pi x\bar{\mu}_3) \approx 0.84(8\pi x\bar{\mu}_3)$.

After including the three-loop corrections to the potential, we find the critical mass and condensates at N^{3}LO and N^{4}LO to be

$$y_{\rm c}|_{\rm N^3LO} = -\frac{x^2}{2^3(4\pi)^2 x}\left[72\ln(x^{\frac{7}{6}}\bar{\mu}_3\pi) - \frac{2337}{16} + 282\ln 2 + \frac{\aleph_{\textcircled{2}}}{2}\right], \tag{37}$$

$$\Delta\langle\Phi^\dagger\Phi\rangle_c|_{\mathrm{N^3LO}} = \frac{x^2}{2^3(4\pi)^2x^2}\left[36\ln x - \frac{1377}{16} + 90\ln 2 + \frac{\aleph_{\text{⚽}}}{2}\right], \tag{38}$$

$$\Delta\langle(\Phi^\dagger\Phi)^2\rangle_c|_{\mathrm{N^3LO}} = \frac{x^2}{2^6(4\pi)^4x^4}\left[120\ln x + 72\ln\pi + \frac{4017}{8} + 372\ln 2 + \aleph_{\text{⚽}}\right], \tag{39}$$

$$y_c|_{\mathrm{N^4LO}} = \frac{x^{\frac{5}{2}}}{2^{\frac{5}{2}}(4\pi)^2x}\left[51\ln x + \frac{1025}{4} + 6\pi^2 + 197\ln 2 - 126\ln 3\right], \tag{40}$$

$$\Delta\langle\Phi^\dagger\Phi\rangle_c|_{\mathrm{N^4LO}} = -\frac{x^{\frac{5}{2}}}{2^{\frac{7}{2}}(4\pi)^2x^2}\left[255\ln x + \frac{4715}{4} + 30\pi^2 + 985\ln 2 - 630\ln 3\right], \tag{41}$$

$$\Delta\langle(\Phi^\dagger\Phi)^2\rangle_c|_{\mathrm{N^4LO}} = -\frac{x^{\frac{5}{2}}}{2^{\frac{9}{2}}(4\pi)^4x^4}\left[102\ln x + \frac{2671}{8} + 12\pi^2 + 394\ln 2 - 252\ln 3\right], \tag{42}$$

where the constant term $\aleph_{\text{⚽}}$ is given in Eq. (16).

Note, that the scalar condensates are renormalization-scale invariant at every order. Furthermore, the scale dependence of y_c is fully consistent with the exact β-function given in Eq. (9). Here, in its dimensionless form, using $\partial_{t_3} \equiv \partial_{\ln\mu_3}$,

$$\beta_y = \partial_{t_3} y = \frac{1}{(4\pi)^2}\frac{3}{16}(17 + 48x - 64x^2). \tag{43}$$

The above expressions mark the *final* result obtainable within perturbation theory since four-loop calculations are nonperturbative [54,60,65].

For the critical mass and the two condensates, we contrast our perturbative results with lattice simulations [32,72,90–92] in Figs. 2 and 3. All three quantities display a marked improvement at small x; this is especially poignant for $\Delta\langle(\Phi^\dagger\Phi)^2\rangle$. However, for $\Delta\langle\Phi^\dagger\Phi\rangle$, the perturbative prediction at NLO appears to agree best with the lattice data and only at very low x, higher-orders become the most accurate predictions; see [93] for a similar trend in the Abelian Higgs model. As a consequence of including the final perturbative corrections, the departure of perturbation theory from lattice data is delayed until $x \sim 0.04$–0.05. A subsequent breakdown of perturbation theory is indeed expected as a second-order transition takes place at $x = x_* = 0.0983(13)$ [90,91].

To illustrate the perturbative uncertainty at each order, we varied the renormalization scale in Fig. 2, in the range $\bar{\mu}_3/(2m_A) = [10^{-\frac{1}{2}}, 10^{\frac{1}{2}}]$. An optimized value for $\bar{\mu}_3$ can be found à la principle of *minimal sensitivity* [52,94,95].

IV. IMPACT ON GRAVITATIONAL WAVES

To investigate the importance of three-loop corrections, we apply the results of Sec. III to a four-dimensional parent theory that maps into Eq. (1) in the high-temperature limit. For maximal freedom of the analysis, we treat our setup as a toy model for gravitational waves from a purely dark sector [96], and do not assume the Standard Model field content. To this end, we assume a SU(2) gauge theory with a scalar doublet Φ and an additional scalar singlet S. The model definition and its mapping into the thermal EFT are detailed in Appendix C.

Pressure (p). To derive the relevant equilibrium thermodynamic quantities for GW production, we construct

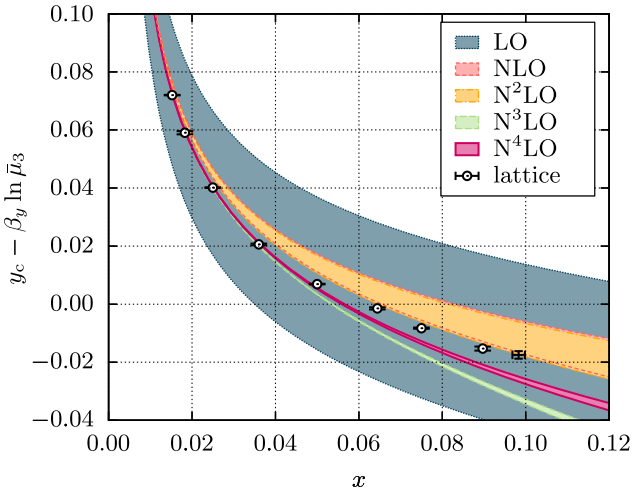

FIG. 2. The renormalization-scale invariant quantity $y_c - \beta_y \ln\bar{\mu}_3$, where y_c is the critical mass, $\bar{\mu}_3$ is the renormalization scale, and β_y is the β-function for y from Eq. (43). Theoretical uncertainties for lattice data from [32,72,90–92] are shown as error bars, uncertainties for the perturbative calculations are shown as error bands by varying $\bar{\mu}_3/(2m_A) = [10^{-\frac{1}{2}}, 10^{\frac{1}{2}}]$. The line of first-order phase transitions ends in a second-order transition at $x \sim 0.1$, indicated by the rightmost lattice point. The orders NLO and N^{2}LO are almost identical.

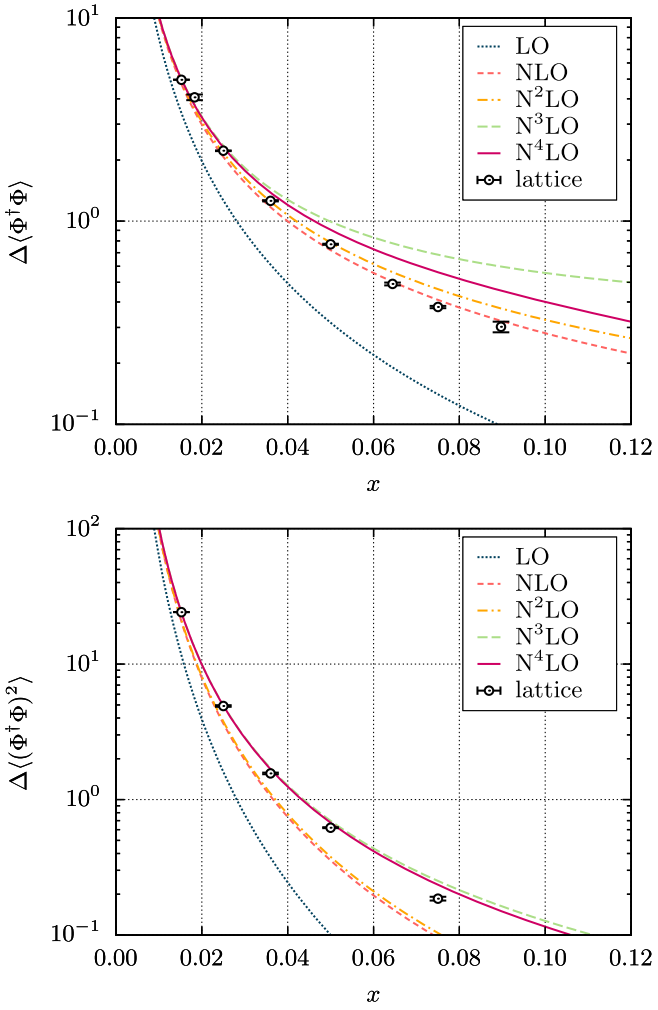

FIG. 3. The jumps in the quadratic $\Delta\langle(\Phi^\dagger\Phi)\rangle$ and quartic $\Delta\langle(\Phi^\dagger\Phi)^2\rangle$ scalar condensates as functions of x, computed in the x-expansion and on the lattice. Both condensates are manifestly gauge and renormalization-scale invariant. The lattice data is taken from [32,72,90–92].

the pressure in the high-temperature expansion. It is composed as

$$p = p_0 - TV_{\text{eff}}, \tag{44}$$

where V_{eff} is the effective potential of the 3D EFT computed in Sec. II, separately for different phases. The unit operator p_0, or the field-independent pressure [25], comes from thermal corrections to the vacuum. From the pressure, we can find the enthalpy $\omega \equiv Tp'$, the speed of sound $c_s^2 \equiv p'/e'$, and the energy density $e = Tp' - p$, where we use the shorthand $p' \equiv \mathrm{d}p/\mathrm{d}T$.

To keep the discussion simple, we regroup the different perturbative orders of the pressure as "1-loop," "2-loop," and "3-loop." A detailed composition of different perturbative orders of the pressure is given in Appendix C 6.

We consider two scenarios for the dark-sector model:

(A) If the singlet is weakly coupled to a light doublet, the doublet can undergo a first-order phase transition while the singlet decouples.
(B) Even if the doublet is too heavy to accommodate a phase transition, a transition can be catalyzed if the interaction with the singlet is sufficiently strong. Here, we will work in a mass regime that admits integrating out the singlet such that only the doublet remains in the EFT.

By focusing on option (A), we fix the parameters of the parent theory (defined in Appendix C 1) to

$$g^2 = 0.5, \qquad \lambda_\phi = 0.0075, \qquad M_\phi = 10\sqrt{2}, \qquad \text{(BM-A)}$$

(in arbitrary units of mass) and assume a simple tree-level relation $\mu_\phi^2 = -M_\phi^2/2$ between the doublet mass parameter and the pole mass. This follows our general strategy, that the 3D EFT computation is at its final perturbative order while zero temperature $\overline{\text{MS}}$ relations are kept minimal, in our toy model. [5] The ratio $\lambda_\phi/g^2 = 0.015$ is the leading, temperature-independent contribution to the dimensionless variable x that controls the behavior of the EFT. In our analysis, we employ the power counting $\lambda_\phi \sim g^3$ since it seems like a natural choice given the formal limit $g^4 \ll \lambda_\phi \ll g^2$ [97].

We illustrate the pressure as a function of temperature in Fig. 4 (top) and normalize the pressure in both phases by the one-loop symmetric-phase pressure. Two-loop corrections affect the pressure at the 1% level, and subsequent three-loop corrections affect the pressure at at the 0.1% level, indicating excellent convergence.

Critical temperature (T_c). The critical temperature T_c, at each order, corresponds to the temperatures where the pressure-difference of the phases vanishes. For (BM-A) the critical temperatures are listed in Table I and depicted by the three rightmost vertical lines of Fig. 4. Since the broken-phase pressure has the symmetric-phase pressure subtracted, the pressure vanishes exactly at the critical mass $y_c(x_c)$ at each order.[6]

In the temperature window of Fig. 4, the critical $x_c \approx 0.021$, as contributions of temporal scalars slightly increase the value of x from its leading value set by

[5]To reach maximal perturbative accuracy in terms of 4D parameters (in realistic models), one also needs to improve the relations between physical observables and $\overline{\text{MS}}$ parameters beyond tree-level [27]. In our toy model, this is not necessary as computing its thermodynamics in terms of $\overline{\text{MS}}$ parameters is identical, regardless of the accuracy of $\overline{\text{MS}}$ parameters and physical observables.

[6]For determining T_c, we employ the *mixed method* of [74]. Therein, only the effective potential is expanded in strict perturbation theory. For T_c, we do *not* perform a strict expansion directly since a similar fully strict expansion for the phase transition strength, α, would become a functionally formidable task.

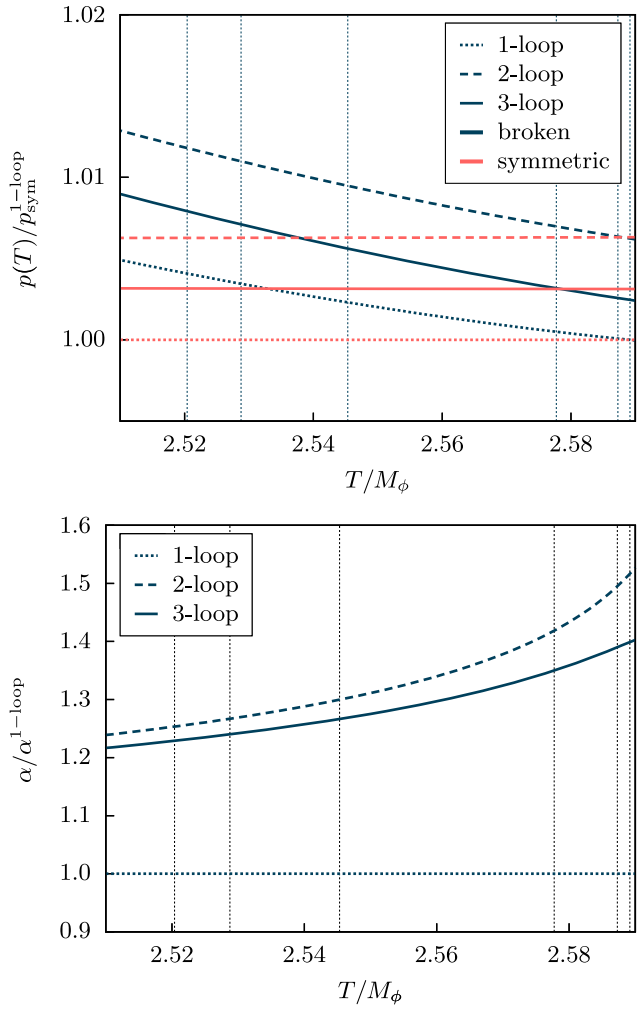

FIG. 4. Pressure (top) and phase-transition strength (bottom) as function of temperature T (scaled by scalar mass M_ϕ) in a benchmark point (BM-A). From left to right, vertical lines indicate the nucleation temperatures and critical temperatures of Table I.

TABLE I. The critical temperature $T_{\rm c}$ and percolation temperature $T_{\rm p}$ in units of the scalar mass M_ϕ for benchmark point (BM-A) at different perturbative orders.

	$T_{\rm c}$
1-loop	2.589
2-loop	2.587
3-loop	2.578
	$T_{\rm p}$
LO	2.545
NLO	2.529
$\rm N^2LO$	2.520

$\lambda_\phi/g^2 = 0.015$; see Appendix C. Since also $T^2/M_\phi^2 \sim 6$, the high-temperature expansion is applicable.

We have verified that points with smaller (larger) λ_ϕ/g^2 lead to increased (decreased) convergence in perturbation theory. Benchmark point (BM-A) illustrates such generic trends.

Phase transition strength (α). The convergence of the pressure is inherited by all quantities further derived from it. One such quantity is the phase transition strength defined via [98,99]

$$\alpha = \frac{\Delta\bar{\theta}}{3\omega_{\rm sym}} = \frac{1}{3p'_{\rm sym}}\left(\frac{\Delta V_{\rm eff}}{c^2_{s,\rm bro}} - \Delta\frac{{\rm d}V_{\rm eff}}{{\rm d}\ln T}\right), \tag{45}$$

where $\omega_{\rm sym}$ is the enthalpy of the symmetric phase, the pseudotrace anomaly is $\bar{\theta} \equiv e - p/c^2_{s,\rm bro}$ and where we used the notation $\Delta p \equiv p|_{\rm bro} - p|_{\rm sym} = -T\Delta V_{\rm eff}$.

In Fig. 4 (bottom), we depict the relative-to-leading-order convergence of α, in analogy to Fig. 4 (top). For the pressure, the relative difference between different loop orders are minute due to the dominating unit operator p_0. Since α depends on the pressure *difference*, it is independent of p_0. Conversely, for α, relative differences between one- and two-loop level can reach 10%, while the difference between two- and three-loop level displays great convergence.

Speed of sound (c_s). While α is dominated by the second, derivative, term in Eq. (45), the term proportional to $\Delta V_{\rm eff}$ is subdominant. This term also depends on the broken-phase speed of sound which is plotted in Fig. 5. The symmetric-phase result is very close to the LO result $c_s^2 = 1/3$ at all orders. The broken-phase speed of sound significantly deviates from this LO value but quickly converges with the loop order. Such deviations can be important for analyses of hydrodynamic properties of the phase transition as they could affect the shape of the GW signal and suppress it by an order of magnitude [98,99]. A careful computation of the speed of sound is required especially for theories whose particle content deviates strongly from the Standard Model one [100]. The *article* at hand completes the perturbative determination of the speed of sound.

Bubble nucleation rate (Γ). Both Figs. 4 and 5 depict the results for the bubble nucleation temperature, given by the three leftmost vertical lines from Table I. These results are obtained by directly following [101,102]; see also [28,103–107]. Here, we merely summarize the rationale for completeness. The bubble nucleation rate can be approximated by $\Gamma \simeq \frac{\kappa}{2\pi}\Sigma$, where the dynamical prefactor κ depends on dissipative processes [108]. Its statistical part Σ can be computed within the 3D EFT as

$$\Sigma \approx [\det_S] e^{-S_B(x,y)}, \tag{46}$$

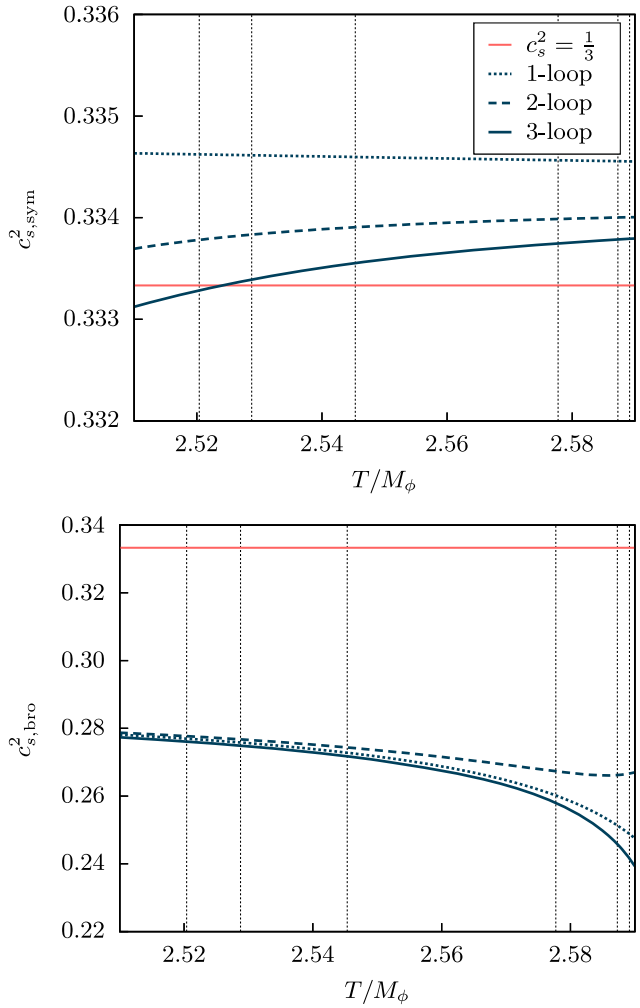

FIG. 5. As Fig. 4 but depicting the speed of sound squared, c_s^2, as a function of temperature for the symmetric (top) and broken (bottom) phase.

where S_B is the bounce action and higher-order corrections are described by the determinant $[\det_S]$. Henceforth, we simply work in approximations that ignore the dynamical prefactor κ [109].

In the 3D EFT, Σ depends only on x, y and we can formally write the statistical part of the rate as an exponential $\exp(-S_B + \ln[\det_S]) \equiv \exp(-S_{\mathrm{eff}})$, and further find the effective action in a strict expansion

$$S_{\mathrm{eff}} = S_{\mathrm{LO}} + xS_{\mathrm{NLO}} + x^{\frac{3}{2}}S_{\mathrm{NNLO}} + \ldots. \tag{47}$$

Here, the powers of x merely indicate the suppression relative to LO.[7] Expressions for each order can be found in [102]. In analogy with Sec. II, integer powers of x come from integrating out vector bosons (in the UV), while fractional powers come from scalar fluctuations (in the IR).

[7]The vector-contribution to the effective action can be expressed with a derivative expansion as $\nabla^2\phi \sim m_{\mathrm{H}}^2\phi \ll m_{\mathrm{A}}^2\phi$.

To relate the statistical S_{eff} to cosmology and the temperature evolution of the universe, we can approximate the condition for successful percolation after bubble nucleation as

$$S_{\mathrm{eff}}(x, y_{\mathrm{p}}) \simeq F[H(T_{\mathrm{p}})], \tag{48}$$

where F is a function of the Hubble parameter $H(T)$. The exact form of F can be found in [72,110,111], but here we approximate it as a constant $F[H(T_{\mathrm{p}})] \approx 126$, which corresponds to about two-thirds of the universe being in the broken phase [111]. We remark that several definitions of T_{p} appear in the literature [10,12,112], and subtleties concerning this reference temperature for GW production were recently discussed in [113,114].

Given $S_{\mathrm{eff}}(x, y_{\mathrm{p}}) \equiv 126$, we can (numerically) find $y_{\mathrm{p}}(x)$ as a curve in the (x, y)-plane. For any parameter point of a parent theory, the percolation temperature T_{p} is given by the condition $y(x(T_{\mathrm{p}})) = y_{\mathrm{p}}(x)$.[8] This is analogous to finding the critical temperature from the condition $y(x(T_{\mathrm{c}})) = y_{\mathrm{c}}(x)$ [32].

In perturbation theory, we can find the LO result from $y(x(T_{\mathrm{p}}^{\mathrm{LO}})) = y_{\mathrm{p}}^{\mathrm{LO}}(x)$ where $y_{\mathrm{p}}^{\mathrm{LO}}$ is determined by S_{LO}. The higher-order corrections $T_{\mathrm{p}}^{\mathrm{NLO}}$ and $T_{\mathrm{p}}^{\mathrm{N^2LO}}$ are then found in a strict perturbative expansion, as detailed in [102]. In Figs. 4 and 5, we observe that in (BM-A), the percolation and critical temperatures are rather close. This is a generic feature of this EFT where percolation occurs with relatively little supercooling below the critical temperature.

While for the critical temperature, we found all results including corrections up to and including N^{4}LO, the strict expansion for the percolation temperature is performed only for the first three orders. The two remaining orders for the bubble nucleation rate are promoted to future work.

Inverse duration (β/H). Another important thermal parameter for GW production is the inverse duration of the transition, defined as

$$\frac{\beta}{H} = -\frac{\mathrm{d}\ln\Gamma}{\mathrm{d}\ln T}. \tag{49}$$

For the benchmark point (BM-A) of Figs. 4 and 5, we report the values listed in Tab. II for the phase transition strength, α, and the inverse duration $\frac{\beta}{H}$ at $T = T_{\mathrm{p}}$.[9]

Higher-order corrections increase α and the overall convergence is good, while they decrease $\frac{\beta}{H_{\mathrm{p}}}$ and convergence is less pronounced, even for the relatively small value of $x \approx 0.021$ of (BM-A). The underlying perturbative computation of the bubble nucleation rate breaks

[8]As [72], we employ y_{p} which is the "nucleation mass" y_{n} of [102].

[9]For $\frac{\beta}{H_{\mathrm{p}}}$, we determine the first three orders in strict perturbative expansion as described in [102].

TABLE II. The phase transition strength, α, and inverse duration $\frac{\beta}{H_\mathrm{p}}$ for the benchmark point (BM-A) of Figs. 4 and 5. Percolation temperatures correspond to Table I.

$\alpha^{1-\mathrm{loop}}(T_\mathrm{p}^{\mathrm{LO}})$	0.014
$\alpha^{2-\mathrm{loop}}(T_\mathrm{p}^{\mathrm{NLO}})$	0.020
$\alpha^{3-\mathrm{loop}}(T_\mathrm{p}^{\mathrm{N^2LO}})$	0.021
$\left(\frac{\beta}{H_\mathrm{p}}\right)_{\mathrm{LO}}$	13578
$\left(\frac{\beta}{H_\mathrm{p}}\right)_{\mathrm{NLO}}$	7182
$\left(\frac{\beta}{H_\mathrm{p}}\right)_{\mathrm{N^2LO}}$	4329

down for $x > 0.058$ [102]. We have verified improved convergence for parameter points that map into smaller values of x. Furthermore, we have verified that the aforementioned trends for α and $\frac{\beta}{H_\mathrm{p}}$ also hold for other parameter points.

Gravitational waves. After detailing several phase transition thermodynamic quantities over a range of temperatures, we now emulate a scan over the model parameter space, typically performed in studies of cosmological phase transitions in beyond the Standard Model theories or dark sectors; cf. [10] and references therein. Along the lines of [10], we recast our scan results in the $(\alpha, \beta/H)$-plane in Fig. 6 for the benchmark point (BM-A), varying $\lambda_\phi \in [0.001, 0.03]$ which corresponds to $x \in [0.006, 0.068]$ within the EFT. For illustration, we show tentative sensitivity regions of LISA and DECIGO in analogy with [115].[10] While none of the transitions have sufficiently large timescales for LISA to probe them,[11] DECIGO and other future GW observatories could observe a primordial GW echo from a dark sector phase transition such as those analyzed here.

Parameter points with small λ_ϕ result in small x, which provide the largest (smallest) value for α_p (β/H_p) toward the bottom right. Even for the smallest values of x, perturbative corrections to β/H_p are sizeable. When x increases, the perturbative computation for the inverse duration breaks completely, as indicated by the deviation of different orders toward the top left. Encouragingly, perturbation theory behaves best toward and within the DECIGO sensitivity, and a total breakdown of perturbation theory occurs only for weaker transitions, which is to be expected.

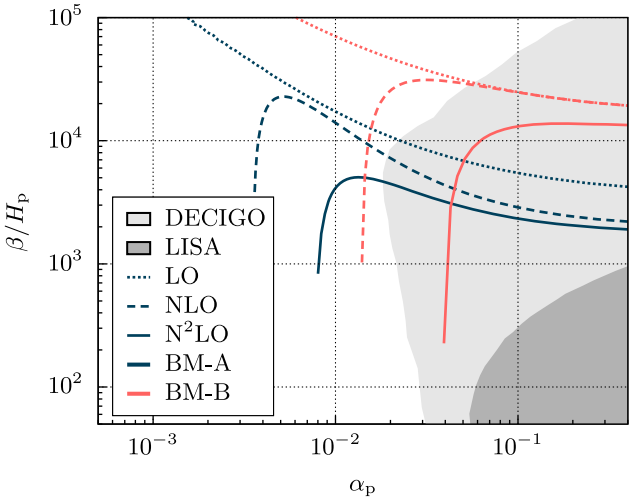

FIG. 6. Connecting our thermal computation to experimental probes via the $(\alpha_\mathrm{p}, \beta/H_\mathrm{p})$-plane by projecting results for benchmark points (BM-A) but by varying $\lambda_\phi \in [0.0001, 0.03]$ ($x \in [0.0054, 0.068]$) and (BM-B) by varying $\lambda_m \in [2, 2.55]$ ($x \in [0.017, 0.098]$). Also shown are the tentative sensitivity regions for LISA [10] and DECIGO [15]. For these curves, x decreases from left to right. For large x, the perturbative expansion for the bubble nucleation rate breaks down, resulting in tails of rapidly falling β/H_p.

In Fig. 6 and in addition to the benchmark point (BM-A) (blue), we also report on another benchmark point (BM-B) (red), *viz.*

$$g^2 = 0.9, \qquad \lambda_s = 1.0, \qquad \sin\theta = 0.2,$$
$$\frac{M_\phi}{\mathrm{GeV}} = 125, \qquad \frac{M_s}{\mathrm{GeV}} = 325, \qquad \frac{v_0}{\mathrm{GeV}} = 246, \qquad \text{(BM-B)}$$

where parameters are defined in Appendix C 1. This scenario emulates the Standard Model augmented with a new scalar field. By design, the singlet is sufficiently heavy to be integrated out from the final EFT; see Appendix C. This serves as an illuminating example that the 3D EFT of SU(2) with a doublet is an invaluable tool for studying the thermodynamics of electroweak-like first-order phase transitions in the presence of field content beyond the dynamical degrees of freedom of the final EFT [33,38,50,118–121].

V. DISCUSSION

This study delivers the final verdict of perturbation theory on electroweak gauge-Higgs theories at high temperature. By accounting for three-loop contributions, any further study perforce requires nonperturbative analyses due to the Linde problem. This *article* builds upon the recent formulation of the re-reorganized perturbative

[10]For connecting with LISA-generation experimental probes [116], we henceforth assume the scalar mass M_ϕ and all other dimensionful quantities in units of GeV. The tentative integrated sensitivity regions at a wall velocity $v_w = 0.95$ for LISA at SNR $= 5$ [117] with $\mathcal{T} = 4$ year mission duration [10] and DECIGO with the *Correlation* design [15] were taken from [115].

[11]This result is expected since phase transitions that map into he 3D EFT of SU(2) with a doublet are not observable by LISA [50].

expansion [73]. While [73] computed its first three orders, here we deliver the remaining two perturbative orders and herald the culmination of a three-decade program initiated by [71,97] for the perturbative analysis of cosmological and electroweak phase transitions in particular.

A similar perturbative completion was previously only achieved for pure scalar theory and QCD at high temperatures. For both theories, perturbative results are in remarkable agreement with nonperturbative lattice Monte-Carlo analyses [52,65]. In turn, for electroweak gauge-Higgs theories, we find remarkable agreement between perturbation theory and lattice simulations by reorganizing the perturbative expansion. This provides additional evidence that the Linde problem is of minor significance in cosmological phase transitions driven by a fundamental scalar field.

Naturally, the precision of our perturbative results diminishes as we approach the critical point. At this juncture, the transition becomes second-order and subsequently evolves into a crossover. Perturbation theory is inherently unreliable for such weak transitions. One estimate suggests that perturbation theory can be trusted for positive critical masses, y_c. However, once y_c turns negative, a second-order transition is expected within perturbation theory.

The perturbative toolbox completed in this *article* readily generalizes to more complicated theories with multiple scalar fields [74]. Thus, computing large perturbative higher-order corrections can follow the methodology outlined in this *article*. In particular, by utilizing the general mass hierarchy between the broken-phase vector bosons and the light transitioning scalar(s), we reorganized the theory to all perturbative orders.

For predictions of a stochastic GW background from a dark sector phase transition, we found that higher-order perturbative corrections ensure a well-controlled perturbation theory for equilibrium thermodynamics. However, the remaining significant uncertainty stems from the current inability to determine the bubble nucleation rate with similar precision. The extension of our findings to more complicated and widely studied theories with nonminimal scalar sectors, and their implications for collider phenomenology and GW predictions, is left to future studies.

Outlook. With the perturbative program now completed, there is ample opportunity for future lattice studies. While perturbation theory can reliably predict the properties of strong transitions, it falls short in describing weak transitions where nonperturbative effects are large. To reliably rule out the possibility of a first-order transition, nonperturbative lattice analyses are essential. These analyses are particularly important for the phenomenological study of extensions of the Standard Model [53] and understanding their potential signatures at future colliders [122]. To this end, not only deciding the phase-transition character with lattice techniques is important, also future simulations for bubble nucleation [72,103,109,123] and sphaleron rates [124–126] are required.

To further enhance precision in understanding cosmological phase transitions, we consider the following future directions:

- At $\mathcal{O}(g^6)$, additional contributions arise in the dimensional reduction via higher-dimensional operators within the 3D EFT. While evaluated for the pure gauge sector of QCD [127], accurately determining their effect in generic theories remains important for probing the validity of the 3D EFT. This validity forms a backbone not only for perturbative, but also lattice studies.
- Purely perturbative $\mathcal{O}(g^6)$ contributions from the hard scale could still be computed for the symmetric-phase pressure; cf. progress in hot QCD [128].
- Building on [102,129], the final perturbative corrections for the thermal bubble nucleation rate and the phase transition duration are yet to be computed. They still source one of the largest uncertainties for predicting GW signals from cosmological phase transitions.

ACKNOWLEDGMENTS

We are grateful to Oliver Gould, Joonas Hirvonen, Maciej Kierkla, Johan Löfgren, Lauri Niemi, Daniel Schmitt, Bogumiła Świeżewska, Van Que Tran, Jorinde van de Vis, Yanda Wu, and Guotao Xia for discussions as this project was carried out. The work of A. E. has been supported by the Swedish Research Council, Project No. VR:2021-00363. P. S. was support by the Swiss National Science Foundation (SNF) under Grant No. PZ00P2-215997 and the Deutsche Forschungsgemeinschaft (DFG, German Research Foundation) through the CRC-TR 211 "Strong-interaction matter under extreme conditions"—Project No. 315477589—TRR 211. P. S. acknowledges the hospitality of CERN during the final stages of this work. T. T. was supported under National Natural Science Foundation of China Grant No. 12375094.

APPENDIX A: EXPANSION OF BROKEN PHASE EFFECTIVE POTENTIAL IN TERMS OF EFT MATCHING

This Appendix illustrates the organization of the perturbative series of Fig. 1 for the broken-phase effective potential, in terms of an EFT matching between the mass scale of the vector bosons and the scale of the phase transition. By adopting the terminology of [74], these scales are dubbed *soft* and *supersoft*.

The supersoft scale EFT is constructed by integrating out the soft scale. The resulting action is

$$S^{\text{tree}}_{\text{supersoft}} = \int_{\mathbf{x}} \frac{1}{2}(\partial_i s)^2 Z_s + \underbrace{\quad\bullet\quad + \bigcirc\quad}_{\text{LO}}$$
$$+ \underbrace{\quad\bigcirc\cdots\bigcirc\quad}_{\text{NLO}} \qquad \text{(A1)}$$
$$+ \underbrace{\quad\bigcirc\cdots\bullet\quad}_{\text{N}^3\text{LO}},$$

where the summation over the s soft scalar fields is implied. The construction of the EFT action follows a standard EFT matching computation using the background-field method [81–83]; see also [130] for an intuitive explanation. In this framework, the strategy is to integrate only over soft, UV, momenta and expand the propagators in supersoft, IR, scalar masses before integration.

Hence, scalar propagators are treated as massless and their mass effect is included as a perturbative two-point interaction, presented as a blob at N^{4}LO in Eq. (A1). These two-point interaction vertices appear at two-loop level, and are effectively counted as three-loop diagrams. The field normalization factor Z_s, resulting from the soft gauge field modes, is computed at one-loop order; see, e.g., [105]. Pure scalar-field diagrams vanish in dimensional regularization given that no scales appear in the propagators. They do not contribute to the matching. However, scalar-field loops are computed within the supersoft EFT in the IR, and at one-loop order are

$$S^{\text{1-loop}}_{\text{supersoft}} = \underbrace{\bigcirc}_{\text{N}^2\text{LO}} + \underbrace{\bigcirc\!\!-\!\!\bigcirc}_{\text{N}^4\text{LO}}, \qquad \text{(A2)}$$

where the "x-expansion" is enforced by treating higher-order contributions (in powers of x) to the scalar mass as perturbative corrections. These corrections are denoted by a blob insertion of Π_ϕ; see Eq. (18). A box denotes the insertion of the two-point vertex $\bar{\Pi}_\phi$ arising from field renormalization; see Eq. (22). Two-loop diagrams within the supersoft EFT are of higher order than N^{4}LO and can thus be omitted in our computation. Combining the results for the soft expansion of Eq. (A1) and the supersoft corrections in Eq. (A2), yields the perturbative expansion of the broken-phase effective potential in Fig. 1.

APPENDIX B: THERMODYNAMICS OF U(1) + HIGGS THEORY

The three-dimensional theory action of the Abelian Higgs model is given by Eq. (1) and its tree-level potential by Eq. (2) where the scalar Φ transforms under U(1). This model has previously been studied in [131–136]. Contrary to the SU(2) model, there is no magnetic mass for the photon. Thus making four-loop computations tractable; at least in principle. However, a nonperturbative mass exists for finite lattice spacings [137,138], and topological effects such as vortices are relevant [139–141]. In the context of SU(2)+ adjoint Higgs theory, similar effects were recently discussed in [142].

For the symmetric phase, the first two orders $V_{\text{eff}}|^{\text{sym}}_{\text{LO}} = V_{\text{eff}}|^{\text{sym}}_{\text{NLO}} \equiv 0$. The first nonvanishing contributions arise at N^{3}LO and N^{4}LO,

$$V_{\text{eff}}\big|^{\text{sym}}_{\text{N}^2\text{LO}} = -\frac{1}{6\pi}(m_3^2)^{\frac{3}{2}}, \qquad \text{(B1)}$$

$$V_{\text{eff}}\big|^{\text{sym}}_{\text{N}^3\text{LO}} = -\frac{g_3^2 m_3^2}{(4\pi)^2}\frac{1}{2}\left[-3 + 4\ln 2 + 2\ln\frac{m_3^2}{\bar{\mu}_3^2}\right], \qquad \text{(B2)}$$

$$V_{\text{eff}}\big|^{\text{sym}}_{\text{N}^4\text{LO}} = \frac{g_3^4}{(4\pi)^3}\frac{(m_3^2)^{\frac{1}{2}}}{12} \times \left[97 + 4\pi^2 - 136\ln 2 - 24\ln\frac{m_3^2}{\bar{\mu}_3^2}\right], \qquad \text{(B3)}$$

computed in general R_ξ (or Fermi) gauge.

The broken-phase effective potential amounts to

$$V_{\text{eff}}\big|^{\text{bro}}_{\text{LO}} = \frac{1}{2}m_3^2\phi^2 + \frac{1}{4}\lambda_3\phi^4 - \frac{1}{6\pi}g_3^3\phi^3, \qquad \text{(B4)}$$

$$V_{\text{eff}}\big|^{\text{bro}}_{\text{NLO}} = \frac{g_3^4\phi^2}{(4\pi)^2}\left[-1 - 2\ln\frac{\bar{\mu}_3}{2g_3\phi}\right], \qquad \text{(B5)}$$

$$V_{\text{eff}}\big|^{\text{bro}}_{\text{N}^2\text{LO}} = -\frac{1}{12\pi}\left[\tilde{m}_h^3 + \tilde{m}_{\text{G}}^3\right], \qquad \text{(B6)}$$

$$V_{\text{eff}}\big|^{\text{bro}}_{\text{N}^3\text{LO}} = \frac{4g_3^2}{(16\pi)^2}\left[m_3^2\left(3 + 4\ln 2 + 8\ln\frac{\bar{\mu}_3}{2g_3\phi}\right) + \lambda_3\phi^2\left(7 + 4\ln 2 + 16\ln\frac{\bar{\mu}_3}{2g_3\phi}\right)\right] + \frac{g_3^5\phi}{(16\pi)^3}\frac{16}{3}[77 + 4\pi^2 - 104\ln 2], \qquad \text{(B7)}$$

$$V_{\text{eff}}\big|^{\text{bro}}_{\text{N}^4\text{LO}} = -\frac{g_3}{(16\pi)^2}\frac{1}{\phi}\frac{4}{3}\left[11\tilde{m}_h^3 + 16\tilde{m}_{\text{G}}^3\right] + \frac{2g_3^4}{(4\pi)^3}\left[-\tilde{m}_h + (\tilde{m}_h + \tilde{m}_{\text{G}})\ln\frac{\bar{\mu}_3}{2g_3\phi}\right], \qquad \text{(B8)}$$

computed in Landau gauge.

The perturbative results of the critical mass and condensates for this model up to N^{2}LO, are

$$y_c = \frac{1}{2(3\pi)^2 x}\left[1 + \frac{9}{2}x\ln\tilde{\mu}_3 - \left(\frac{x}{2}\right)^{\frac{3}{2}}\right], \tag{B9}$$

$$\Delta\langle\Phi^\dagger\Phi\rangle_c = \frac{1}{2(3\pi)^2 x^2}\left[1 - \frac{9}{2}x + \frac{25}{2}\left(\frac{x}{2}\right)^{\frac{3}{2}}\right], \tag{B10}$$

$$\Delta\langle(\Phi^\dagger\Phi)^2\rangle_c = \frac{1}{2^2(3\pi)^4 x^4}\left[1 - 9x + 13\left(\frac{x}{2}\right)^{\frac{3}{2}}\right], \tag{B11}$$

where $\tilde{\mu}_3 \equiv e^{\frac{1}{2}+\ln\frac{3}{2}}(\pi x\bar{\mu}_3)$. After including three-loop corrections, we find the critical mass and condensates at N^{3}LO and N^{4}LO to be

$$y_c|_{\mathrm{N^3LO}} = -\frac{x^2}{2^3(4\pi)^2 x}\left[64\ln\left(x^{\frac{9}{8}}\bar{\mu}_3\pi\right) + 63 + 4\pi^2 - 152\ln 2 + 64\ln 3\right], \tag{B12}$$

$$\Delta\langle\Phi^\dagger\Phi\rangle_c|_{\mathrm{N^3LO}} = \frac{x^2}{2^3(4\pi)^2 x^2}\left[24\ln x + 111 + 4\pi^2 - 104\ln 2\right], \tag{B13}$$

$$\Delta\langle(\Phi^\dagger\Phi)^2\rangle_c|_{\mathrm{N^3LO}} = \frac{x^2}{2^6(3\pi)^4 x^4}\left[216\ln x + \frac{1755}{2} + 18\pi^2 - 576\ln 2 + 144\ln(3\pi)\right], \tag{B14}$$

$$y_c|_{\mathrm{N^4LO}} = -\frac{x^{\frac{5}{2}}}{2^{\frac{5}{2}}(4\pi)^2 x}\left[12\ln x - \frac{85}{6} - 2\pi^2 + 32\ln 2\right], \tag{B15}$$

$$\Delta\langle\Phi^\dagger\Phi\rangle_c|_{\mathrm{N^4LO}} = \frac{x^{\frac{5}{2}}}{2^{\frac{7}{2}}(4\pi)^2 x^2}\left[60\ln x - \frac{143}{2} - 10\pi^2 + 160\ln 2\right], \tag{B16}$$

$$\Delta\langle(\Phi^\dagger\Phi)^2\rangle_c|_{\mathrm{N^4LO}} = \frac{x^{\frac{5}{2}}}{2^{\frac{9}{2}}(3\pi)^4 x^4}\left[54\ln x - \frac{1341}{8} - 9\pi^2 + 144\ln 2\right]. \tag{B17}$$

APPENDIX C: THERMAL EFT FOR SU(2) WITH A DOUBLET AND SINGLET DARK SECTOR

This Appendix details the model employed in Sec. IV. While most of the results can be extracted from the literature [27,39,40,100,118], we include and display novel thermal corrections.

1. Model at zero temperature

We define our setup through the Lagrangian

$$\mathcal{L} = \frac{1}{4}F^a_{\mu\nu}F^a_{\mu\nu} + (D_\mu\Phi)^\dagger(D_\mu\Phi) + \frac{1}{2}(\partial_\mu S)^2 + V(\Phi, S), \tag{C1}$$

where the covariant derivative $D_\mu\Phi = (\partial_\mu - igA_\mu)\Phi$, where $A_\mu = A^a_\mu T^a$. The scalar potential is

$$V(\Phi,S) = m_\phi^2\Phi^\dagger\Phi + \lambda_\phi(\Phi^\dagger\Phi)^2 + \frac{1}{2}m_s^2S^2 + \frac{1}{4}\lambda_s S^4 + \frac{1}{2}\mu_m(\Phi^\dagger\Phi)^2 S + \frac{1}{2}\lambda_m(\Phi^\dagger\Phi)^2S^2 + \mu_1 S + \frac{1}{3}\mu_3 S^3. \tag{C2}$$

The cubic portal allows for doublet-singlet mixing. We work in a parametrization where the mixing angle $\sin\theta$, the scalar mass squared eigenvalues M_ϕ^2, M_s^2,[12] the doublet vacuum expectation value (VEV) at zero temperature v_0, the gauge coupling g^2, the singlet self interactions λ_s, μ_3, and the portal coupling λ_m are treated as input parameters. We fix the singlet VEV to vanish which fixes singlet tadpole coupling $\mu_1 = -\mu_m v_0^2/4$. Concretely, we use the tree-level relations

$$\begin{aligned} m_\phi^2 &= -\frac{1}{4}\left(M_\phi^2 + M_s^2 + (M_\phi^2 - M_s^2)\cos(2\theta)\right), \\ m_s^2 &= \frac{1}{2}\left(-\lambda_m v_0^2 + M_\phi^2 + M_s^2 - (M_\phi^2 - M_s^2)\cos(2\theta)\right), \\ \lambda_\phi &= \frac{1}{4v_0^2}\left(M_\phi^2 + M_s^2 + (M_\phi^2 - M_s^2)\cos(2\theta)\right), \\ \mu_m &= -\frac{2}{v_0}\left(M_\phi^2 - M_s^2\right)\sin\theta\cos\theta. \end{aligned} \tag{C3}$$

[12]For a small mixing angle $\sin\theta \ll 1$, the mass M_ϕ describes the *mostly* doublet and M_s the *mostly* singlet state.

For a realistic theory, instead of a dark-sector toy setup, it would be warranted to improve these relations by the corresponding zero-temperature one-loop corrections [27], cf. [40].

2. Effective theory

At high temperatures $m_\phi^2/T, m_s^2/T \sim g \ll 1$ and the 3D zero Matsubara modes live in the IR at the soft scale $|p| \sim \mathcal{O}(gT)$. In turn, the nonzero Matsubara modes in the UV at scale $|p| \sim \mathcal{O}(\pi T)$ can be integrated out [143]. The resulting 3D EFT is of the same functional form as Eq. (C1) with the addition of the Lagrangian for the temporal component of the gauge field

$$\mathcal{L}^{\rm 3d}_{\rm temporal} = \frac{1}{2}(D_r A_0^a)^2 + \frac{1}{2}m_{\rm D}^2 A_0^a A_0^a + \frac{1}{4}\kappa_3 (A_0^a A_0^a)^2 + \frac{1}{2}h_3 \phi^\dagger \phi A_0^a A_0^a + \frac{1}{4}y_3 S^2 A_0^a A_0^a + \frac{1}{2}x_3 S^2 A_0^a A_0^a, \tag{C4}$$

where the covariant derivative for triplet SU(2) temporal scalars, reads $D_r A_0^a = \partial_r A_0^a + g_3 \epsilon^{abc} A_r^b A_0^c$. Here, we chose different normalizations for h_3 [12,27], y_3, and x_3 compared to [39]. In addition, $\kappa_3 \equiv 2\lambda_{\rm VLL}[1]$ compared to the convention used by `DRalgo`; see the `dark-su2-higgs-singlet.m` model file [144].

In analogy to Eq. (A1), the construction of the EFT can be schematically illustrated in terms of the effective action as

$$S_{\rm EFT}[\varphi] = \int_{\mathbf{x}} \frac{1}{2}(\partial_i \varphi)^2 Z_\varphi + \bullet + \bigcirc + \ominus$$

$$= \int_{\mathbf{x}} \Big\{ p_0^{\varphi=0} + \Big[\blacksquare\!\!-\!\!\bullet\!\!- + \blacksquare\!\!-\!\!(1)\!\!- + -\!\!(2)\!\!- \Big] + \Big[\diagup\!\!\bullet\!\!\diagdown + \diagup\!\!(1)\!\!\diagdown \Big] + \Big[-\!\!(1)\!\!- \Big] \Big\}$$

$$= \int_{\mathbf{x}} \Big\{ \underbrace{p_0^{\varphi=0} + \frac{1}{2}\varphi^2(m_3^2) + \frac{1}{4}\varphi^4(\lambda_3)}_{\mathcal{O}(g^4)} + \mathcal{O}(g^6\varphi^6) \Big\}, \tag{C5}$$

where encircled numbers indicate the loop order and boxes indicate kinetic insertions on external lines in analogy with Eq. (21). Here, the effective action is computed using the background field method, in terms of a formal scalar background field φ. For simplicity, we present here only one such background field, keeping in mind that for multiple scalar fields within the EFT, each field has its own background. Furthermore, in this simplified illustration, we do not detail the background field method for the gauge sector.

In the first line of Eq. (C5), loop diagrams involving Matsubara sum-integrals are integrated over the hard momenta, i.e., over nonzero Matsubara modes in the UV. Masses $M^2(\varphi)$ in propagators depend on the background field, and sum-integrals are computed in the high-temperature expansion of $M^2/T^2 \sim g^2$. Matsubara zero modes in the IR are treated as massless. The field normalization factor

$$Z_\varphi = 1 + \frac{\mathrm{d}}{\mathrm{d}k^2}\Big[-\!\!\bigcirc\!\!- \Big], \tag{C6}$$

is likewise obtained by integrating over nonzero Matsubara modes, and computing the relevant scalar two-point functions in an expansion of soft external momenta k.

In the second line of Eq. (C5), we have expanded the action in terms of background field, φ. We have highlighted that the unit operator p_0 is field-independent, and return to its computation below. Terms with nonvanishing background field correspond to Green's functions generated by the effective action, and the ellipsis denotes eight- and higher-point correlators.

In the third line of Eq. (C5), we identify these Green's functions with EFT parameters of the scalar potential, that we denote by a schematic m_3^2 and λ_3 for this simplified illustration. We remark, that in the second line, the effect of the Z-factor is captured by the Green's functions[13] which is illustrated by a box on the external lines. In practice, the 3D parameter matching relations can be determined by directly computing Green's functions without the presence of the background field, instead of computing the action. This is practical, especially for the gauge, and gauge-scalar mixed sectors [27].

Assuming a power counting in which the parent theory squared mass parameters are soft $\sim(gT)^2$, in the high-T expansion and the quartic couplings scale as $\mathcal{O}(g^2)$, allows for determining all 3D EFT parameters at $\mathcal{O}(g^4)$ provided that the masses are determined at two-loop and couplings at one-loop level. Sextic and higher operators can be neglected as they contribute at $\mathcal{O}(g^6)$.

Within the so-far constructed EFT, the Debye mass $m_{\rm D}^2$ is soft, and parametrically larger than the mass of the scalar doublet Φ that undergoes the transition deeper in the IR. This allows to integrate out the temporal scalar A_0^a, to build an EFT at a *softer* scale. In addition, we assume that the singlet mass $m_s \sim m_{\rm D}$, and hence the singlet is integrated out as well. The resulting EFT in the IR is given by Eq. (1).

Constructing this softer EFT aligns with Eq. (C5) with a few modifications. In this case, only the soft loops of the temporal scalar and the singlet are integrated over, while the doublet (as well as spatial gauge field) are treated as

[13] Z-factor contributions are crucial to obtain a renormalization-scale invariant, gauge-independent result [12,105].

massless. The convergence of the soft theory is slower as each new loop order is suppressed by g, whereas in the hard-to-soft matching, the loop suppression is g^2. Typically, in softer theory only one-loop effects from the soft scale are included for the scalar quartic coupling [27]. While this is numerically an excellent approximation for contributions of the temporal scalar, for the singlet, also two-loop effects can be sizable. Similarly, effects from the soft singlet can induce sizable corrections to the sextic operator, to which soft contributions in general are parametrically $\mathcal{O}(g^3)$ [27]. While at first glance this might seem alarming, we comment on these issues in Sec. C 5 when we present concrete expressions and further discuss our numerical analysis.

The unit operator in the final EFT composes of $p_0 = p_{\mathrm{E}} + p_{\mathrm{M}}$ [77], where hard and soft contributions, typically labeled as electrostatic (p_{E}) and magnetic (p_{M}), follow from vacuum diagrams of the form (here in four-dimensional units)

$$p_{\mathrm{E}} = \quad + \quad + \quad \sim T^4\left(g^0 + g^2 + g^4 + \mathcal{O}(g^6)\right), \tag{C7}$$

$$p_{\mathrm{M}} = T\Big(\quad + \quad + \quad \Big) \sim T^4\left(g^3 + g^4 + g^5 + \mathcal{O}(g^6)\right), \tag{C8}$$

where each loop order is represented by its most complicated topology.

For p_{E}, the loop integration is over nonzero Matsubara modes and each order is suppressed by g^2. For p_{M}, loops involve soft fields and each order is suppressed by g. In both cases, all contributions are purely perturbative and for hot QCD, the computation of the four-loop $\mathcal{O}(g^6)$ has recently been organized at the level of master integrals [128].

3. Collection of expressions

This section collects all relevant thermal corrections for the softer EFT. Installing the power counting

$$m_\phi^2, m_s^2 \sim (gT)^2, \qquad \lambda_\phi, \lambda_s, \lambda_m \sim g^2, \qquad \mu_3, \mu_m \sim g^2 T, \tag{C9}$$

leads to a similar EFT construction as in [40], and the hard-to-soft matching relations can be read from therein (by omitting U(1), SU(3), and fermionic sectors contributions). Alternatively, one can compute the parameters using `DRalgo` [41] via the model file [144]. Hence, we do not list these relations here.

The matching results in the two-loop mass parameters (and singlet tadpole) and one-loop couplings. Such relations are renormalization-scale invariant at $\mathcal{O}(g^4)$, and in our numerical analysis, we apply one-loop β-functions to run parameters to the optimal thermal scale $\bar{\mu}_{\mathrm{opt}} = 4\pi e^{-\gamma_{\mathrm{E}}} T$ [71], where γ_{E} is the Euler-Mascheroni constant. Since the required β-functions can be obtained with `DRalgo`, we do not list them explicitly.

If the singlet decouples, we need smaller doublet self-coupling which satisfies the parametric scaling $\lambda_\phi \sim g^3/\pi$; cf. (BM-A). Also in this case, we include $\mathcal{O}(\lambda_\phi^2)$ terms in the hard-to-soft matching, yet remark that these contributions, as well as $\mathcal{O}(g^2\lambda_\phi)$, are miniscule compared to pure gauge contributions of $\mathcal{O}(g^4)$ that dominate.

In (BM-B), and by further fixing $\lambda_m = 2.5$ in this section, we find that λ_ϕ, λ_m, λ_s, and the gauge coupling contribute with approximately equal importance to the two-loop thermal mass parameters, while the effect from cubic couplings is less important.[14] Cubic couplings, however, yield the largest (one-loop) correction for the singlet tadpole which is dominated by its tree-level value while two-loop corrections are further suppressed. For both mass parameters, tree-level and one-loop contributions are dominant while the two-loop correction is subdominant. This indicates a controlled high-T expansion, and concretely $m_\phi^2/T \sim 1/4$ and $m_s^2/T \sim 4/5$ in vicinity of critical temperature $T_{\mathrm{c}} \sim 188$ GeV.

The unit operator for the hard modes from Eq. (C7) and the soft modes from Eq. (C8), can be obtained with `DRalgo` and reads

$$\begin{aligned} p_{\mathrm{E}} = {} & 11\frac{\pi^2}{90}T^4 - \frac{T^2}{576}\left(T^2(39g^2 + 24\lambda_\phi + 4\lambda_m + 3\lambda_s) + 24\left(4m_\phi^2 + m_s^2\right)\right) \\ & + \frac{T^2}{(4\pi)^2}\left[\frac{m_s^2}{24}L_b(2\lambda_m + 3\lambda_s) + m_\phi^2\left(L_b\left(\lambda_\phi + \frac{1}{12}\lambda_m\right) + \frac{g^2}{8}\left(-2 + 12\ln(2\pi) - 12(\ln\zeta_2)' + 9L_b\right)\right)\right. \\ & \left. - \frac{1}{48}(4\mu_3^2 + 3\mu_m^2)(2\ln(2\pi) - 2(\ln\zeta_2)' + L_b)\right] - \frac{L_b}{(4\pi)^2}\left(\mu_\phi^4 + \frac{1}{4}\mu_s^4\right) \\ & + \frac{T^2}{(4\pi)^2}\left[\alpha_{\mathrm{E}g^4}g^4 + \alpha_{\mathrm{E}\lambda_\phi g^2}\lambda_\phi g^2 + \alpha_{\mathrm{E}\lambda_\phi^2}\lambda_\phi^2 + \alpha_{\mathrm{E}\lambda_m g^2}\lambda_m g^2 + \alpha_{\mathrm{E}\lambda_\phi\lambda_m}\lambda_\phi\lambda_m + \alpha_{\mathrm{E}\lambda_m^2}\lambda_m^2 + \alpha_{\mathrm{E}\lambda_m\lambda_s}\lambda_m\lambda_s + \alpha_{\mathrm{E}\lambda_s^2}\lambda_s^2\right], \end{aligned} \tag{C10}$$

[14] Contributions of μ_3, μ_m to one-loop thermal masses are $\propto L_b$ and vanish at the optimized $\bar{\mu}_{\mathrm{opt}} = 4\pi e^{-\gamma_{\mathrm{E}}} T$. Further corrections to the matching relations from these couplings are $\propto \zeta_3/(4\pi)^4$ or $\zeta_5/(4\pi)^6$ and we find them to be negligible; cf. Sec. 4.2 of [39].

$$\frac{p_{\rm M}}{T} = -\frac{1}{12\pi}\left(3m_{\rm D}^3 + m_{s,3}^3\right) - \frac{1}{(4\pi)^2}\left[g_3^2 m_{\rm D}^2\left(\frac{9}{2} + 6\ln\frac{\bar{\mu}_3}{2m_{\rm D}}\right) + \frac{3}{4}\left(5\kappa_3 m_{\rm D}^2 + \lambda_{s,3}m_{s,3}^2\right)\right] - \frac{2m_{\rm D}}{(4\pi)^3}\left[g_3^4(23+\pi^2-11\ln 2) + 12h_3^2 + \frac{9}{8}\left(g_3^4 + 8h_3^2\right)\ln\frac{\bar{\mu}_3}{2m_{\rm D}}\right], \tag{C11}$$

where $L_b \equiv 2\ln\frac{\bar{\mu}e^{\gamma_{\rm E}}}{4\pi T}$, $\zeta_n = \zeta(n)$ is the Riemann zeta function, and $(\ln\zeta_n)' \equiv \zeta'(n)/\zeta(n)$. For the T^4-coefficients, we adopted the (slightly modified) notation of [78,100], and results for these coefficients can also be read from therein. In fact, the term proportional to κ_3 in Eq. (C11) is $\mathcal{O}(g^6T^4)$ and could hence be dropped. In the three-loop contribution, however, we have included only the temporal scalar contribution, as these can be conveniently read from [77], but not the singlet contributions which are currently beyond reach for the fangs of `DRalgo`.

Corrections from different loop orders to $p_0 = p_{\rm E} + p_{\rm M}$ with respect to its LO result are listed in Table III. For (BM-A), and as already highlighted above, these corrections are dominated by pure gauge contributions, and corrections involving λ_ϕ and m_ϕ^2/T^2 are minor. Also for (BM-B), these relative corrections display great convergence, albeit not as good as in (BM-A).

The explicit "soft-to-softer" EFT matching relations, where the temporal scalar and the singlet are integrated out, read

$$\bar{g}_3^2 = g_3^2 - \left[\frac{1}{24\pi}\frac{g_3^4}{m_{\rm D}}\right], \tag{C12}$$

$$\bar{\lambda}_{\phi,3} = \lambda_{\phi,3} - \left[\frac{1}{32\pi}\left(\frac{3h_3^2}{m_{\rm D}} + \frac{\lambda_{m,3}^2}{m_{s,3}}\right)\right] + \frac{1}{(4\pi)^2}\left[\frac{1}{m_{\rm D}^2}\left(\frac{3}{4}h_3^3 - \frac{3}{2}h_3^2 g_3^2 + \frac{3}{8}h_3 g_3^4 - \frac{3}{128}g_3^6\right) + \frac{1}{4}\frac{\lambda_{m,3}^3}{m_{s,3}^2}\right] + \Gamma_3, \tag{C13}$$

TABLE III. Corrections to the unit operator $p_0 = p_{\rm E} + p_{\rm M}$ with respect to its LO result for benchmark points (BM-A) and (BM-B) originating from soft and hard modes.

BM-A	Hard	Soft
1-loop		1.60%
2-loop	1.7%	0.32%
3-loop	0.9%	0.30%
BM-B	**Hard**	**Soft**
1-loop		8.7%
2-loop	6.9%	1.7%
3-loop	3.3%	0.1%[a]

[a]This number is only for temporal mode contributions as singlet terms were omitted as described earlier.

$$\bar{m}_{\phi,3}^2 = m_{\phi,3}^2 - \left[\frac{1}{8\pi}\left(3h_3 m_{\rm D} + \lambda_{m,3}m_{s,3}\right)\right] - \frac{1}{(4\pi)^2}\left[\frac{3}{4}h_3^2 - \frac{15}{4}h_3\kappa_3 - \frac{3}{2}h_3 g_3^2 - \frac{3}{4}\lambda_{m,3}\lambda_{s,3} + \left(\frac{3}{2}h_3^2 - 6h_3 g_3^2 + \frac{3}{4}g_3^4\right)\ln\frac{\bar{\mu}_3}{2m_{\rm D}} + \frac{1}{4}\lambda_{m,3}^2\left(1 + 2\ln\frac{\bar{\mu}_3}{2m_{s,3}}\right)\right] + \Pi_3. \tag{C14}$$

Here, we have included two-loop contributions to the self-coupling. While these corrections are often omitted, they are formally of the same order as the two-loop thermal mass. They can readily be found using the two-loop effective potentials computed in [40,51].

The contributions of the singlet cubic couplings are

$$\Gamma_3 = \frac{1}{4}\mu_{1,3}\left(2\frac{\lambda_{m,3}\mu_{m,3}}{m_{s,3}^4} - \frac{\mu_{3,3}\mu_{m,3}^2}{m_{s,3}^6}\right) - \frac{\mu_{m,3}^2}{8m_{s,3}^2} + \frac{\mu_{m,3}^2}{32\pi m_{s,3}^5}\left(\frac{5}{4}\mu_{m,3}^2 - \mu_{m,3}\mu_{3,3} - \mu_{3,3}^2\right) + \frac{\mu_{m,3}^2}{32\pi m_{s,3}^3}\left(5\lambda_{m,3} - 12\lambda_{\phi,3} - 3\lambda_{s,3} - 2\frac{\lambda_{m,3}\mu_{3,3}}{\mu_{m,3}}\right) - \frac{1}{48(4\pi)^2 m_{s,3}^4}\left(4\mu_{3,3}^2 + 3\mu_{m,3}^2\right) - \frac{\lambda_{\phi,3}}{24\pi}\frac{\mu_{m,3}^2}{m_{s,3}^3}, \tag{C15}$$

$$\Pi_3 = -\frac{\mu_{1,3}\mu_{m,3}}{2m_{s,3}^2} + \frac{\mu_{m,3}}{16\pi m_{s,3}}\left(2\mu_{3,3} - \mu_{m,3}\right) + \frac{\mu_{1,3}}{32\pi}\left[\frac{\mu_{m,3}^2}{m_{s,3}^5}\left(\mu_{m,3} - 2\mu_{3,3}\right) + \frac{4\lambda_{m,3}}{m_{s,3}^3}\left(2\mu_{m,3} + \mu_{3,3}\right)\right] + \frac{\lambda_{m,3}}{24(4\pi)^2 m_{s,3}^2}\left(4\mu_{3,3}^2 + 3\mu_{m,3}^2\right) - \frac{m_{\phi,3}^2}{48\pi}\frac{\mu_{m,3}^2}{m_{s,3}^3}. \tag{C16}$$

Our computation of these contributions is diagrammatic [118] and involves a class of one-particle-reducible (1PR) diagrams as detailed therein. We, however, integrate out the singlet at the soft scale, whereas in [118] the singlet is integrated out along with nonzero Matsubara modes. Consequently the integrals associated with the required diagrams are different. We have included the 1PR contributions at tree- and one-loop level but omitted them at two-loop level. There, we only include one-particle-irreducible (1PI) contributions. These 1PI contributions can be found using the two-loop effective potential [40,51].

In addition, we have included the leading contribution from the one-loop Z-factor induced by the singlet, described by the very last terms in Eqs. (C15) and (C16).

In (BM-B), in which $m_{\rm D}/T \sim 4/5$ and $m_{s,3}/T \sim 4/3$ in vicinity of $T_{\rm c}$ and where integrating out the singlet is justified, we find that the dominant effect in Γ_3 and Π_3 comes from the tree-level terms. The one-loop contributions $\propto 1/\pi$ are subdominant while two-loop as well as Z-factor contributions are negligible.

4. How a singlet catalyzes strong transitions

A relatively heavy singlet with sufficiently strong portal interaction to the doublet can enhance the transition strength by reducing the effective quartic coupling for the doublet

$$x \equiv \frac{\bar{\lambda}_{\phi,3}}{\bar{g}_3^2} \approx \frac{1}{\bar{g}_3^2}\left(\lambda_{\phi,3} + \frac{\mu_{1,3}\lambda_{m,3}\mu_{m,3}}{2m_{s,3}^4} - \frac{\mu_{m,3}^2}{8m_{s,3}^2} - \frac{\lambda_{m,3}^2}{32\pi m_{s,3}}\right). \tag{C17}$$

Here, we only kept terms that produce a significant effect, i.e., tree-level cubic contributions (for simplicity, we omitted terms $\propto \mu_3$) and one-loop Z_2-symmetric contributions.[15] When the singlet tadpole $\mu_{1,3}$ is negative, all singlet effects in Eq. (C17) come with opposite sign compared to $\lambda_{\phi,3}$, and hence *reduce* x. The presence of cubic couplings ease the realization of this effect significantly as their effect appears already at tree-level. In Eq. (C15), we carefully inspected that higher-order corrections preserve this effect. In general, two-loop effects to Eq. (C17) tend to come with positive sign, and hence diminish the effect of reducing the effective doublet self-interaction.

To further understand the role of the singlet in a doublet-driven phase transition, it is illuminating to consider the soft-to-softer EFT construction as follows. The one-loop contribution to the effective potential from the soft modes are

$$V_{\rm eff}(\varphi) = \frac{1}{2}m_{\phi,3}^2\varphi^2 + \frac{1}{4}\lambda_{\phi,3}\varphi^4 - \frac{1}{16\pi}g_3^3\varphi^3 - \frac{1}{12\pi}\left(3\left(m_{\rm D}^2 + \frac{1}{2}h_3\varphi^2\right)^{\frac{3}{2}} + \left(m_{s,3}^2 + \frac{1}{2}\lambda_{m,3}\varphi^2\right)^{\frac{3}{2}}\right), \tag{C18}$$

where we neglected the singlet cubic couplings for simplicity. The last three terms are contributions of the vector boson, temporal scalar, and the singlet, with masses

$$m_{\rm A}^2 = \frac{g_3^2\varphi^2}{4}, \qquad m_{\rm A_0}^2 = m_{\rm D}^2 + \frac{1}{2}h_3\varphi^2, \qquad m_S^2 = m_{s,3}^2 + \frac{1}{2}\lambda_{m,3}\varphi^2, \tag{C19}$$

respectively. The essence of the softer EFT construction is the mass hierarchy $m_{\rm A}^2 \ll m_{\rm A_0}^2, m_S^2$ which holds for field values toward the symmetric phase where the background field vanishes. In the broken phase, expansions in $h_3\varphi^2/m_{\rm D}^2$ and $\lambda_{m,3}\varphi^2/m_{s,3}^2$ yield the one-loop contributions in Eqs. (C13) and (C14). From Eq. (C13), it is evident that a larger portal interaction leads to a smaller effective quartic coupling of the transitioning field, and therefore smaller x, allowing to strengthen the transition.

For the temporal scalar, this expansion is always sensible, as the Debye mass $m_{\rm D}$ is always soft as there is no negative zero temperature contributions that could make it smaller. For the singlet $m_{s,3}^2 \sim m_s^2 + g^2T^2$, and the situation is different, since m_s^2 could be negative.[16] In that case, it is possible that $m_{s,3}^2 \ll \frac{1}{2}\lambda_{m,3}\varphi^2$ and the singlet shall be treated on same footing as the spatial gauge field. It is not integrated out together with the temporal scalar, but remains in the final EFT and is treated in analogy to the vector boson as described in Appendix A. In this case, the cubic term in the LO potential becomes

$$-\frac{\varphi^3}{16\pi}\left(\bar{g}_3^3 + \frac{\sqrt{2}}{3}\lambda_{m,3}^{\frac{3}{2}}\right) \equiv -\frac{\varphi^3}{16\pi}\eta^3. \tag{C20}$$

We observe, that the singlet can significantly increase the height of the potential barrier generated by the vector boson, and therefore enhance the transition strength. Or in other words, one can define a new, effective $x_{\rm eff} \equiv \bar{\lambda}_{\phi,3}/\eta^2$, where $\eta^2 \equiv (\bar{g}_3^3 + \frac{\sqrt{2}}{3}\lambda_{m,3}^{\frac{3}{2}})^{\frac{2}{3}}$ and larger $\lambda_{m,3}$ lead to smaller $x_{\rm eff}$, and hence stronger transitions. In practical applications, the portal coupling is significantly larger than the gauge coupling. In such a limit, it is really the ratio λ_ϕ/λ_m that controls the perturbative expansion. Indeed, one should always organize the perturbative power counting in terms of the largest dimensionless coupling in a parent theory, in this case λ_m. The setup discussed in this paragraph was recently formulated for general models in [74] up to and including N^{2}LO corrections. With the technology presented in this *article* together with the companion article [1], such computations can be performed at maximal perturbative accuracy.

[15] Subdominant effects come from temporal scalar and two-loop Z_2-symmetric singlet contributions in Eq. (C13) as well as one-loop cubic contributions in Eq. (C15). Effects of two-loop temporal scalars in Eq. (C13) and other cubic contributions in Eq. (C15) are negligible. A similar organization of relative sizes of different contributions holds also for the mass parameter (and hence y); cf. Eqs. (C14) and (C16).

[16] In our numerical study in (BM-B), we ensure that m_s^2 remains positive and sufficiently large to integrate out the singlet.

5. Higher-dimensional operators

Integrating out both the soft temporal scalars and the singlet, induces the following contribution to the doublet higher-dimensional operator[17]

$$\left[c_6+\frac{1}{192\pi}\left(\frac{3h_3^3}{m_{\rm D}^3}+\frac{\lambda_{m,3}^3}{m_{s,3}^3}\right)+\frac{\mu_{m,3}^2}{24}\left(\frac{\lambda_{m,3}}{m_{s,3}^4}-\frac{\mu_{m,3}\mu_{3,3}}{m_{s,3}^6}\right)\right](\Phi^\dagger\Phi)^3. \quad \text{(C21)}$$

Here, $c_6\sim\mathcal{O}(g^6)$ encodes contributions from the hard modes [39]. The remaining terms result from the soft modes, and one-loop contributions scale formally as $\mathcal{O}(g^3/\pi)$ while tree-level cubic terms are even larger, $\mathcal{O}(g^2)$. In practice, contributions from the hard modes and the temporal scalars produce a negligible effect, which is also the case for singlet contributions—despite their formal, parametric counting— provided that the singlet is sufficiently heavy.

We remark, however, that the operator (C21) *cannot* be neglected when $\bar{\lambda}_{\phi,3}$ and hence x become negative in the vicinity of the critical temperature. This commonly occurs in many theories (cf. e.g., [50,119,120]) and happens also in our toy dark sector setup for large (small) portal couplings (singlet masses). For studies in which this higher dimensional operator is kept within the 3D EFT see [12,102] (cf. also [145]).

6. Perturbative expansion

To capture the thermal contributions enhanced in the IR, we have utilized a chain of EFTs starting from the hard (πT) to the soft (gT) to the softer to supersoft ($g^{\frac{3}{2}}/\sqrt{\pi}T$) scale. It is this high tower of effective theories above the nonperturbative, ultrasoft scale ($g^2/\pi T$) that brew the ultimate potion for resummations required to construct the pressure at high temperature.

In terms of the formal power counting of a parent theory, the different contributions to the pressure scale as

$$p\sim T^4\left(\underbrace{\boxed{g^0+g^2+g^3}}_{\text{“1-loop”}}+\underbrace{\boxed{g^4+g^{\frac{9}{2}}}}_{\text{“2-loop”}}+\underbrace{\boxed{g^5+g^{\frac{11}{2}}}}_{\text{“3-loop”}}+\mathcal{O}(g^6)\right). \quad \text{(C22)}$$

[17]Naturally, several higher dimensional operators are generated at the same order. Such operators involve gauge fields and their effect for the phase-transition thermodynamics is often argued to be subdominant compared to the sextic scalar operator.

TABLE IV. Symmetric-phase pressure and free-energy difference relative to their respective leading order for benchmark point (BM-A).

Order	$\frac{p_{\rm sym}}{p_{{\rm sym},g^0}}$	$\frac{\Delta V_{\rm eff}}{\Delta V_{{\rm eff},g^3}}$
g^2	1.72%	
g^3	1.64%	
g^4	0.62%	35.4%
$g^{\frac{9}{2}}$	0.004%	1.4%
g^5	0.31%	24.3%
$g^{\frac{11}{2}}$	0.0001%	1.1%

The coupling orders contributing to the different “loop orders” are convoluted—due to various resummations. We comment on the following subtleties

- 1-loop: The orders $\mathcal{O}(g^0)$ and $\mathcal{O}(g^2)$ only arise in the symmetric phase from hard modes. While the $\mathcal{O}(g^2)$-terms technically originate from two-loop diagrams, it is sensible to group them with the broken-phase LO $\mathcal{O}(g^3)$ soft contributions.
- 2-loop: Terms of $\mathcal{O}(g^4)$ arise from various two-loop diagrams, except for hard contributions in the symmetric phase that appear at three-loop level. Terms of $\mathcal{O}(g^{\frac{9}{2}})$ appear at one-loop, but are be numerically close to $\mathcal{O}(g^4)$ terms.
- 3-loop: Terms of $\mathcal{O}(g^5)$ and $\mathcal{O}(g^{\frac{11}{2}})$ require three-loop computations and are, similar to “2-loop”, numerically almost identical in practice.

Since we do not perform strict expansions for the pressure, the speed of sound, and α, we have found the above grouping of different orders practical for our results in Figs. 4–6. In turn, we do not truncate the effective theory matching relations at “1-loop,” “2-loop,” or “3-loop,” but work with the full relations in all cases. As a consequence, many expressions at higher orders include formally higher-order *tails* in the full EFT spirit.

In (BM-A), for increasing orders in g in Eq. (C22), we find for the symmetric-phase pressure that corrections relative to its leading $\mathcal{O}(g^0)$ appear with the importance listed in Table IV. The same table also lists the corrections for the broken-phase pressure $p_{\rm bro}=p_{\rm sym}-T\Delta V_{\rm eff}$ and free-energy difference, relative to its leading contribution at $\mathcal{O}(g^3)$. Since these numbers depend on the value of T at which the pressure is evaluated, they are taken to be tentative. In particular, we find that “supersoft” corrections with fractional powers are minute, despite their apparent counting. For this reason, we group them together with integer power orders as in Eq. (C22). Similar observations also hold for (BM-B) which we do not illustrate separately.

[1] A. Ekstedt, P. Schicho, and T. V. I. Tenkanen (to be published).
[2] A. H. Guth, The inflationary universe: A possible solution to the horizon and flatness problems, Phys. Rev. D **23**, 347 (1981).
[3] A. Achúcarro *et al.*, Inflation: Theory and observations, arXiv:2203.08128.
[4] V. A. Rubakov and M. E. Shaposhnikov, Electroweak baryon number nonconservation in the early universe and in high-energy collisions, Usp. Fiz. Nauk **166**, 493 (1996).
[5] D. E. Morrissey and M. J. Ramsey-Musolf, Electroweak baryogenesis, New J. Phys. **14**, 125003 (2012).
[6] D. Bödeker and W. Buchmüller, Baryogenesis from the weak scale to the grand unification scale, Rev. Mod. Phys. **93**, 035004 (2021).
[7] C. J. Hogan, Gravitational radiation from cosmological phase transitions, Mon. Not. R. Astron. Soc. **218**, 629 (1986).
[8] C. Caprini, R. Durrer, and G. Servant, Gravitational wave generation from bubble collisions in first-order phase transitions: An analytic approach, Phys. Rev. D **77**, 124015 (2008).
[9] M. Hindmarsh, S. J. Huber, K. Rummukainen, and D. J. Weir, Numerical simulations of acoustically generated gravitational waves at a first order phase transition, Phys. Rev. D **92**, 123009 (2015).
[10] C. Caprini *et al.*, Detecting gravitational waves from cosmological phase transitions with LISA: An update, J. Cosmol. Astropart. Phys. 03 (2020) 024.
[11] P. Athron, C. Balázs, A. Fowlie, L. Morris, and L. Wu, Cosmological phase transitions: From perturbative particle physics to gravitational waves, Prog. Part. Nucl. Phys. **135**, 104094 (2024).
[12] D. Croon, O. Gould, P. Schicho, T. V. I. Tenkanen, and G. White, Theoretical uncertainties for cosmological first-order phase transitions, J. High Energy Phys. 04 (2021) 055.
[13] P. Amaro-Seoane *et al.* (LISA Collaboration), Laser interferometer space antenna, arXiv:1702.00786.
[14] H. Kudoh, A. Taruya, T. Hiramatsu, and Y. Himemoto, Detecting a gravitational-wave background with next-generation space interferometers, Phys. Rev. D **73**, 064006 (2006).
[15] S. Kawamura *et al.*, The Japanese space gravitational wave antenna: DECIGO, Classical Quantum Gravity **28**, 094011 (2011).
[16] K. Yagi and N. Seto, Detector configuration of DECIGO/BBO and identification of cosmological neutron-star binaries, Phys. Rev. D **83**, 044011 (2011).
[17] X. Gong *et al.*, Descope of the ALIA mission, J. Phys. Conf. Ser. **610**, 012011 (2015).
[18] J. Luo *et al.* (TianQin Collaboration), TianQin: A space-borne gravitational wave detector, Classical Quantum Gravity **33**, 035010 (2016).
[19] M. Quiros, Finite temperature field theory and phase transitions, in *ICTP Summer School in High-Energy Physics and Cosmology* (1999), pp. 187–259, arXiv: hep-ph/9901312.
[20] C. Grojean and G. Servant, Gravitational waves from phase transitions at the electroweak scale and beyond, Phys. Rev. D **75**, 043507 (2007).
[21] C. Delaunay, C. Grojean, and J. D. Wells, Dynamics of non-renormalizable electroweak symmetry breaking, J. High Energy Phys. 04 (2008) 029.
[22] S. Profumo, M. J. Ramsey-Musolf, and G. Shaughnessy, Singlet Higgs phenomenology and the electroweak phase transition, J. High Energy Phys. 08 (2007) 010.
[23] J. R. Espinosa, T. Konstandin, J. M. No, and M. Quiros, Some cosmological implications of hidden sectors, Phys. Rev. D **78**, 123528 (2008).
[24] J. Kehayias and S. Profumo, Semi-analytic calculation of the gravitational wave signal from the electroweak phase transition for general quartic scalar effective potentials, J. Cosmol. Astropart. Phys. 03 (2010) 003.
[25] E. Braaten and A. Nieto, Effective field theory approach to high temperature thermodynamics, Phys. Rev. D **51**, 6990 (1995).
[26] E. Braaten and A. Nieto, Free energy of QCD at high temperature, Phys. Rev. D **53**, 3421 (1996).
[27] K. Kajantie, M. Laine, K. Rummukainen, and M. E. Shaposhnikov, Generic rules for high temperature dimensional reduction and their application to the standard model, Nucl. Phys. **B458**, 90 (1996).
[28] O. Gould and J. Hirvonen, Effective field theory approach to thermal bubble nucleation, Phys. Rev. D **104**, 096015 (2021).
[29] J. Löfgren, Stop comparing resummation methods, J. Phys. G **50**, 125008 (2023).
[30] P. H. Ginsparg, First order and second order phase transitions in gauge theories at finite temperature, Nucl. Phys. **B170**, 388 (1980).
[31] T. Appelquist and R. D. Pisarski, High-temperature Yang-Mills theories and three-dimensional quantum chromodynamics, Phys. Rev. D **23**, 2305 (1981).
[32] K. Kajantie, M. Laine, K. Rummukainen, and M. E. Shaposhnikov, The electroweak phase transition: A non-perturbative analysis, Nucl. Phys. **B466**, 189 (1996).
[33] J. M. Cline and K. Kainulainen, Supersymmetric electroweak phase transition: Beyond perturbation theory, Nucl. Phys. **B482**, 73 (1996).
[34] M. Laine, Effective theories of MSSM at high temperature, Nucl. Phys. **B481**, 43 (1996).
[35] M. Losada, High temperature dimensional reduction of the MSSM and other multiscalar models, Phys. Rev. D **56**, 2893 (1997).
[36] A. Rajantie, SU(5) + adjoint Higgs model at finite temperature, Nucl. Phys. **B501**, 521 (1997).
[37] J. O. Andersen, Dimensional reduction of the two Higgs doublet model at high temperature, Eur. Phys. J. C **11**, 563 (1999).
[38] M. Laine, G. Nardini, and K. Rummukainen, Lattice study of an electroweak phase transition at $m_h \simeq 126$ GeV, J. Cosmol. Astropart. Phys. 01 (2013) 011.
[39] P. M. Schicho, T. V. I. Tenkanen, and J. Österman, Robust approach to thermal resummation: Standard Model meets a singlet, J. High Energy Phys. 06 (2021) 130.

[40] L. Niemi, P. Schicho, and T. V. I. Tenkanen, Singlet-assisted electroweak phase transition at two loops, Phys. Rev. D **103**, 115035 (2021).

[41] A. Ekstedt, P. Schicho, and T. V. I. Tenkanen, DRalgo: A package for effective field theory approach for thermal phase transitions, Comput. Phys. Commun. **288**, 108725 (2023).

[42] M. Lewicki, M. Merchand, L. Sagunski, P. Schicho, and D. Schmitt, Impact of theoretical uncertainties on model parameter reconstruction from GW signals sourced by cosmological phase transitions, Phys. Rev. D **110**, 023538 (2024).

[43] P. Bandyopadhyay and S. Jangid, Discerning singlet and triplet scalars at the electroweak phase transition and gravitational wave, Phys. Rev. D **107**, 055032 (2023).

[44] S. Jangid and H. Okada, Exploring CP-violation in $Y = 0$ inert triplet with real singlet, Phys. Rev. D **108**, 055025 (2023).

[45] L. Niemi and T. V. I. Tenkanen, Investigating two-loop effects for first-order electroweak phase transitions, arXiv:2408.15912.

[46] K. Farakos, K. Kajantie, K. Rummukainen, and M. E. Shaposhnikov, 3-d physics and the electroweak phase transition: A framework for lattice Monte Carlo analysis, Nucl. Phys. **B442**, 317 (1995).

[47] K. Kajantie, M. Laine, K. Rummukainen, and M. E. Shaposhnikov, A Nonperturbative analysis of the finite T phase transition in $\mathrm{SU}(2) \times \mathrm{U}(1)$ electroweak theory, Nucl. Phys. **B493**, 413 (1997).

[48] M. Laine and K. Rummukainen, Two Higgs doublet dynamics at the electroweak phase transition: A non-perturbative study, Nucl. Phys. **B597**, 23 (2001).

[49] K. Kainulainen, V. Keus, L. Niemi, K. Rummukainen, T. V. I. Tenkanen, and V. Vaskonen, On the validity of perturbative studies of the electroweak phase transition in the Two Higgs Doublet model, J. High Energy Phys. 06 (2019) 075.

[50] O. Gould, J. Kozaczuk, L. Niemi, M. J. Ramsey-Musolf, T. V. I. Tenkanen, and D. J. Weir, Nonperturbative analysis of the gravitational waves from a first-order electroweak phase transition, Phys. Rev. D **100**, 115024 (2019).

[51] L. Niemi, M. J. Ramsey-Musolf, T. V. I. Tenkanen, and D. J. Weir, Thermodynamics of a two-step electroweak phase transition, Phys. Rev. Lett. **126**, 171802 (2021).

[52] O. Gould, Real scalar phase transitions: A nonperturbative analysis, J. High Energy Phys. 04 (2021) 057.

[53] L. Niemi, M. J. Ramsey-Musolf, and G. Xia, Nonperturbative study of the electroweak phase transition in the real scalar singlet extended Standard Model, arXiv:2405.01191.

[54] A. D. Linde, Infrared problem in thermodynamics of the Yang-Mills gas, Phys. Lett. **96B**, 289 (1980).

[55] E. V. Shuryak, Theory of hadronic Plasma, Sov. Phys. JETP **47**, 212 (1978).

[56] J. I. Kapusta, Quantum chromodynamics at high temperature, Nucl. Phys. **B148**, 461 (1979).

[57] T. Toimela, The next term in the thermodynamic potential of QCD, Phys. Lett. **124B**, 407 (1983).

[58] P. B. Arnold and C.-X. Zhai, The three loop free energy for pure gauge QCD, Phys. Rev. D **50**, 7603 (1994).

[59] P. B. Arnold and C.-x. Zhai, The three loop free energy for high temperature QED and QCD with fermions, Phys. Rev. D **51**, 1906 (1995).

[60] K. Kajantie, M. Laine, K. Rummukainen, and Y. Schröder, The pressure of hot QCD up to g6 ln(1/g), Phys. Rev. D **67**, 105008 (2003).

[61] A. Gynther, M. Laine, Y. Schröder, C. Torrero, and A. Vuorinen, Four-loop pressure of massless O(N) scalar field theory, J. High Energy Phys. 04 (2007) 094.

[62] J. O. Andersen, L. Kyllingstad, and L. E. Leganger, Pressure to order g^8 log g of massless ϕ^4 theory at weak coupling, J. High Energy Phys. 08 (2009) 066.

[63] A. Hietanen, K. Kajantie, M. Laine, K. Rummukainen, and Y. Schröder, Plaquette expectation value and gluon condensate in three dimensions, J. High Energy Phys. 01 (2005) 013.

[64] F. Di Renzo, M. Laine, V. Miccio, Y. Schröder, and C. Torrero, The Leading non-perturbative coefficient in the weak-coupling expansion of hot QCD pressure, J. High Energy Phys. 07 (2006) 026.

[65] K. Kajantie, M. Laine, K. Rummukainen, and Y. Schröder, Four loop vacuum energy density of the SU(N(c)) + adjoint Higgs theory, J. High Energy Phys. 04 (2003) 036.

[66] K. Kajantie, M. Laine, K. Rummukainen, and M. E. Shaposhnikov, 3-D SU(N) + adjoint Higgs theory and finite temperature QCD, Nucl. Phys. **B503**, 357 (1997).

[67] K. Kajantie, M. Laine, A. Rajantie, K. Rummukainen, and M. Tsypin, The phase diagram of three-dimensional SU(3) + adjoint Higgs theory, J. High Energy Phys. 11 (1998) 011.

[68] K. Kajantie, M. Laine, K. Rummukainen, and Y. Schröder, Four loop logarithms in 3-d gauge + Higgs theory, Nucl. Phys. B, Proc. Suppl. **119**, 577 (2003).

[69] F. Di Renzo, M. Laine, Y. Schröder, and C. Torrero, Four-loop lattice-regularized vacuum energy density of the three-dimensional SU(3) + adjoint Higgs theory, J. High Energy Phys. 09 (2008) 061.

[70] A. Hietanen, K. Kajantie, M. Laine, K. Rummukainen, and Y. Schröder, Three-dimensional physics and the pressure of hot QCD, Phys. Rev. D **79**, 045018 (2009).

[71] K. Farakos, K. Kajantie, K. Rummukainen, and M. E. Shaposhnikov, 3-D physics and the electroweak phase transition: Perturbation theory, Nucl. Phys. **B425**, 67 (1994).

[72] O. Gould, S. Güyer, and K. Rummukainen, First-order electroweak phase transitions: A nonperturbative update, Phys. Rev. D **106**, 114507 (2022).

[73] A. Ekstedt, O. Gould, and J. Löfgren, Radiative first-order phase transitions to next-to-next-to-leading order, Phys. Rev. D **106**, 036012 (2022).

[74] O. Gould and T. V. I. Tenkanen, Perturbative effective field theory expansions for cosmological phase transitions, J. High Energy Phys. 01 (2024) 048.

[75] J. C. Collins and J. A. M. Vermaseren, Axodraw version 2, arXiv:1606.01177.

[76] S. P. Martin and H. H. Patel, Two-loop effective potential for generalized gauge fixing, Phys. Rev. D **98**, 076008 (2018).

[77] A. Gynther and M. Vepsäläinen, Pressure of the standard model near the electroweak phase transition, J. High Energy Phys. 03 (2006) 011.

[78] A. Gynther and M. Vepsäläinen, Pressure of the standard model at high temperatures, J. High Energy Phys. 01 (2006) 060.
[79] M. Laine and M. Meyer, Standard model thermodynamics across the electroweak crossover, J. Cosmol. Astropart. Phys. 07 (2015) 035.
[80] D. J. Broadhurst, A dilogarithmic three-dimensional Ising tetrahedron, Eur. Phys. J. C **8**, 363 (1999).
[81] L. F. Abbott, Introduction to the background field method, Acta Phys. Pol. B **13**, 33 (1982).
[82] A. Denner, G. Weiglein, and S. Dittmaier, Application of the background field method to the electroweak standard model, Nucl. Phys. **B440**, 95 (1995).
[83] B. Henning, X. Lu, and H. Murayama, How to use the standard model effective field theory, J. High Energy Phys. 01 (2016) 023.
[84] V. Shtabovenko, R. Mertig, and F. Orellana, FeynCalc 10: Do multiloop integrals dream of computer codes?, Comput. Phys. Commun. **306**, 109357 (2025).
[85] A. V. Smirnov and M. Zeng, FIRE 6.5: Feynman integral reduction with new simplification library, Comput. Phys. Commun. **302**, 109261 (2024).
[86] B. Ruijl, T. Ueda, and J. Vermaseren, FORM version 4.2, arXiv:1707.06453.
[87] P. Nogueira, Automatic Feynman graph generation, J. Comput. Phys. **105**, 279 (1993).
[88] Y. Schröder and A. Vuorinen, High-precision epsilon expansions of single-mass-scale four-loop vacuum bubbles, J. High Energy Phys. 06 (2005) 051.
[89] K. Kajantie, M. Laine, K. Rummukainen, and Y. Schröder, How to resum long distance contributions to the QCD pressure?, Phys. Rev. Lett. **86**, 10 (2001).
[90] M. Gurtler, E.-M. Ilgenfritz, and A. Schiller, Where the electroweak phase transition ends, Phys. Rev. D **56**, 3888 (1997).
[91] K. Rummukainen, M. Tsypin, K. Kajantie, M. Laine, and M. E. Shaposhnikov, The universality class of the electroweak theory, Nucl. Phys. **B532**, 283 (1998).
[92] M. Laine and K. Rummukainen, What's new with the electroweak phase transition?, Nucl. Phys. B, Proc. Suppl. **73**, 180 (1999).
[93] A. Ekstedt, Lattice vs perturbation theory: Testing the Abelian-Higgs model at three loops (to be published).
[94] P. M. Stevenson, Optimized perturbation theory, Phys. Rev. D **23**, 2916 (1981).
[95] I. Ghisoiu, J. Moller, and Y. Schroder, Debye screening mass of hot Yang-Mills theory to three-loop order, J. High Energy Phys. 11 (2015) 121.
[96] D. Croon, V. Sanz, and G. White, Model discrimination in gravitational wave spectra from dark phase transitions, J. High Energy Phys. 08 (2018) 203.
[97] P. B. Arnold and O. Espinosa, The effective potential and first order phase transitions: Beyond leading-order, Phys. Rev. D **47**, 3546 (1993).
[98] F. Giese, T. Konstandin, and J. van de Vis, Model-independent energy budget of cosmological first-order phase transitions—A sound argument to go beyond the bag model, J. Cosmol. Astropart. Phys. 07 (2020) 057.
[99] F. Giese, T. Konstandin, K. Schmitz, and J. Van De Vis, Model-independent energy budget for LISA, J. Cosmol. Astropart. Phys. 01 (2021) 072.
[100] T. V. I. Tenkanen and J. van de Vis, Speed of sound in cosmological phase transitions and effect on gravitational waves, J. High Energy Phys. 08 (2022) 302.
[101] A. Ekstedt, Higher-order corrections to the bubble-nucleation rate at finite temperature, Eur. Phys. J. C **82**, 173 (2022).
[102] A. Ekstedt, Convergence of the nucleation rate for first-order phase transitions, Phys. Rev. D **106**, 095026 (2022).
[103] G. D. Moore and K. Rummukainen, Electroweak bubble nucleation, nonperturbatively, Phys. Rev. D **63**, 045002 (2001).
[104] J. Löfgren, M. J. Ramsey-Musolf, P. Schicho, and T. V. I. Tenkanen, Nucleation at finite temperature: A gauge-invariant perturbative framework, Phys. Rev. Lett. **130**, 251801 (2023).
[105] J. Hirvonen, J. Löfgren, M. J. Ramsey-Musolf, P. Schicho, and T. V. I. Tenkanen, Computing the gauge-invariant bubble nucleation rate in finite temperature effective field theory, J. High Energy Phys. 07 (2022) 135.
[106] A. Ekstedt, Bubble nucleation to all orders, J. High Energy Phys. 08 (2022) 115.
[107] A. Ekstedt, O. Gould, and J. Hirvonen, BubbleDet: A Python package to compute functional determinants for bubble nucleation, J. High Energy Phys. 12 (2023) 056.
[108] J. S. Langer, Statistical theory of the decay of metastable states, Ann. Phys. (N.Y.) **54**, 258 (1969).
[109] O. Gould, A. Kormu, and D. J. Weir, A nonperturbative test of nucleation calculations for strong phase transitions, arXiv:2404.01876.
[110] K. Enqvist, J. Ignatius, K. Kajantie, and K. Rummukainen, Nucleation and bubble growth in a first order cosmological electroweak phase transition, Phys. Rev. D **45**, 3415 (1992).
[111] J. Ellis, M. Lewicki, and J. M. No, On the maximal strength of a first-order electroweak phase transition and its gravitational wave signal, J. Cosmol. Astropart. Phys. 04 (2019) 003.
[112] H.-K. Guo, K. Sinha, D. Vagie, and G. White, The benefits of diligence: How precise are predicted gravitational wave spectra in models with phase transitions?, J. High Energy Phys. 06 (2021) 164.
[113] P. Athron, C. Balázs, and L. Morris, Supercool subtleties of cosmological phase transitions, J. Cosmol. Astropart. Phys. 03 (2023) 006.
[114] P. Athron, L. Morris, and Z. Xu, How robust are gravitational wave predictions from cosmological phase transitions?, J. Cosmol. Astropart. Phys. 05 (2024) 075.
[115] L. S. Friedrich, M. J. Ramsey-Musolf, T. V. I. Tenkanen, and V. Q. Tran, Addressing the gravitational wave—collider inverse problem, arXiv:2203.05889.
[116] P. Auclair *et al.* (LISA Cosmology Working Group), Cosmology with the laser interferometer space antenna, Living Rev. Relativity **26**, 5 (2023).
[117] P. Amaro-Seoane *et al.* (LISA Collaboration), Laser interferometer space antenna, arXiv:1702.00786.
[118] T. Brauner, T. V. I. Tenkanen, A. Tranberg, A. Vuorinen, and D. J. Weir, Dimensional reduction of the standard

model coupled to a new singlet scalar field, J. High Energy Phys. 03 (2017) 007.
[119] J. O. Andersen, T. Gorda, A. Helset, L. Niemi, T. V. I. Tenkanen, A. Tranberg, A. Vuorinen, and D. J. Weir, Nonperturbative analysis of the electroweak phase transition in the two Higgs doublet model, Phys. Rev. Lett. **121**, 191802 (2018).
[120] L. Niemi, H. H. Patel, M. J. Ramsey-Musolf, T. V. I. Tenkanen, and D. J. Weir, Electroweak phase transition in the real triplet extension of the SM: Dimensional reduction, Phys. Rev. D **100**, 035002 (2019).
[121] T. Gorda, A. Helset, L. Niemi, T. V. I. Tenkanen, and D. J. Weir, Three-dimensional effective theories for the two Higgs doublet model at high temperature, J. High Energy Phys. 02 (2019) 081.
[122] M. J. Ramsey-Musolf, The electroweak phase transition: A collider target, J. High Energy Phys. 09 (2020) 179.
[123] G. D. Moore, K. Rummukainen, and A. Tranberg, Nonperturbative computation of the bubble nucleation rate in the cubic anisotropy model, J. High Energy Phys. 04 (2001) 017.
[124] G. D. Moore, Measuring the broken phase sphaleron rate nonperturbatively, Phys. Rev. D **59**, 014503 (1999).
[125] M. D'Onofrio, K. Rummukainen, and A. Tranberg, Sphaleron rate in the minimal Standard Model, Phys. Rev. Lett. **113**, 141602 (2014).
[126] J. Annala and K. Rummukainen, Electroweak sphaleron in a magnetic field, Phys. Rev. D **107**, 073006 (2023).
[127] M. Laine, P. Schicho, and Y. Schröder, Soft thermal contributions to 3-loop gauge coupling, J. High Energy Phys. 05 (2018) 037.
[128] P. Navarrete and Y. Schröder, The g^6 pressure of hot Yang-Mills theory: Canonical form of the integrand, arXiv: 2408.15830.
[129] O. Gould and T. V. I. Tenkanen, On the perturbative expansion at high temperature and implications for cosmological phase transitions, J. High Energy Phys. 06 (2021) 069.
[130] J. Hirvonen, Intuitive method for constructing effective field theories, arXiv:2205.02687.
[131] M. Karjalainen, M. Laine, and J. Peisa, The order of the phase transition in 3-d U(1) + Higgs theory, Nucl. Phys. B, Proc. Suppl. **53**, 475 (1997).
[132] M. Karjalainen and J. Peisa, Dimensionally reduced U(1) + Higgs theory in the broken phase, Z. Phys. C **76**, 319 (1997).
[133] K. Kajantie, M. Karjalainen, M. Laine, and J. Peisa, Masses and phase structure in the Ginzburg-Landau model, Phys. Rev. B **57**, 3011 (1998).
[134] K. Kajantie, M. Karjalainen, M. Laine, and J. Peisa, Three-dimensional U(1) gauge + Higgs theory as an effective theory for finite temperature phase transitions, Nucl. Phys. **B520**, 345 (1998).
[135] K. Kajantie, M. Laine, T. Neuhaus, A. Rajantie, and K. Rummukainen, Duality and scaling in three-dimensional scalar electrodynamics, Nucl. Phys. **B699**, 632 (2004).
[136] K. Kajantie, M. Laine, T. Neuhaus, A. Rajantie, and K. Rummukainen, Critical behavior of the Ginzburg-Landau model in the type II region, Nucl. Phys. B, Proc. Suppl. **106**, 959 (2002).
[137] T. Banks, R. Myerson, and J. B. Kogut, Phase transitions in Abelian lattice gauge theories, Nucl. Phys. **B129**, 493 (1977).
[138] J. Ambjorn, A. J. G. Hey, and S. Otto, String tensions for lattice gauge theories in $(2 + 1)$-dimensions, Nucl. Phys. **B210**, 347 (1982).
[139] K. Kajantie, M. Karjalainen, M. Laine, J. Peisa, and A. Rajantie, Thermodynamics of gauge invariant U(1) vortices from lattice Monte Carlo simulations, Phys. Lett. B **428**, 334 (1998).
[140] K. Kajantie, M. Laine, T. Neuhaus, J. Peisa, A. Rajantie, and K. Rummukainen, Vortex tension as an order parameter in three-dimensional U(1) + Higgs theory, Nucl. Phys. **B546**, 351 (1999).
[141] K. Kajantie, M. Laine, T. Neuhaus, A. Rajantie, and K. Rummukainen, Statistical mechanics of vortices from field theory, Nucl. Phys. **B559**, 395 (1999).
[142] L. Niemi, K. Rummukainen, R. Seppä, and D. J. Weir, Infrared physics of the 3D SU(2) adjoint Higgs model at the crossover transition, J. High Energy Phys. 02 (2023) 212.
[143] M. Laine and A. Vuorinen, Basics of thermal field theory, Lect. Notes Phys. **925**, 1 (2016).
[144] DRalgo/examples/dark-su2-higgs-singlet.m, https://github.com/DR-algo/DRalgo/blob/main/examples/dark-su2-higgs-singlet.m.
[145] J. E. Camargo-Molina, R. Enberg, and J. Löfgren, A new perspective on the electroweak phase transition in the standard model effective field theory, J. High Energy Phys. 10 (2021) 127.